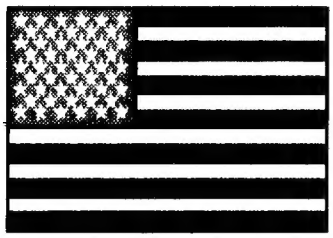

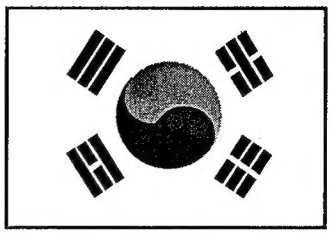

Contract Report SL-95-7
UAST-CR-93-002

JOINT U.S./ROK R&D PROGRAM FOR NEW UNDERGROUND AMMUNITION STORAGE TECHNOLOGIES

FINAL REPORT

INFLUENCE OF GEOMETRIC APPROXIMATIONS ON COMPUTATIONAL RESULTS IN COMPLEX TUNNEL CONFIGURATIONS

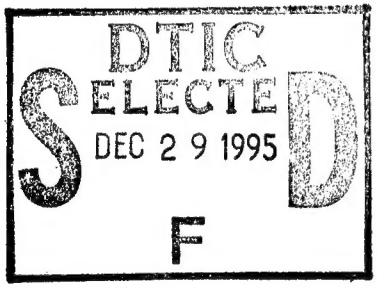

by

Robert G. Ekler
Lynn W. Kennedy
Charles E. Needham

S-Cubed, a Division of Maxwell Laboratories
2501 Yale Boulevard, SE, Suite 300
Albuquerque, New Mexico 87106

September 1995

Prepared for U.S. Army Engineer Waterways Experiment Station
3909 Halls Ferry Road
Vicksburg, Mississippi 39180-6199

PRINTED ON RECYCLED PAPER

Contract Report SL-95-7
September 1995

US Army Corps of Engineers
Waterways Experiment Station

Joint U.S./ROK R&D Program for New Underground Ammunition Storage Technologies

Influence of Geometric Approximations on Computational Results in Complex Tunnel Configurations

by Robert G. Ekler, Lynn W. Kennedy, Charles E. Needham, S-Cubed

WES

Prepared for Headquarters, U.S. Army Corps of Engineers

Joint U.S./ROK R&D Program for New Underground Ammunition Storage Technologies

Contract Report SL-95-7
September 1995

Influence of Geometric Approximations on Computational Results in Complex Tunnel Configurations

by Robert G. Ekler, Lynn W. Kennedy, Charles E. Needham

S-Cubed, Division of Maxwell Laboratories
2501 Yale Boulevard, SE, Suite 300
Albuquerque, NM 87106

Final report

Approved for public release; distribution is unlimited

Prepared for U.S. Army Corps of Engineers
Washington, DC 20314-1000

Monitored by U.S. Army Engineer Waterways Experiment Station
3909 Halls Ferry Road, Vicksburg, MS 39180-6199

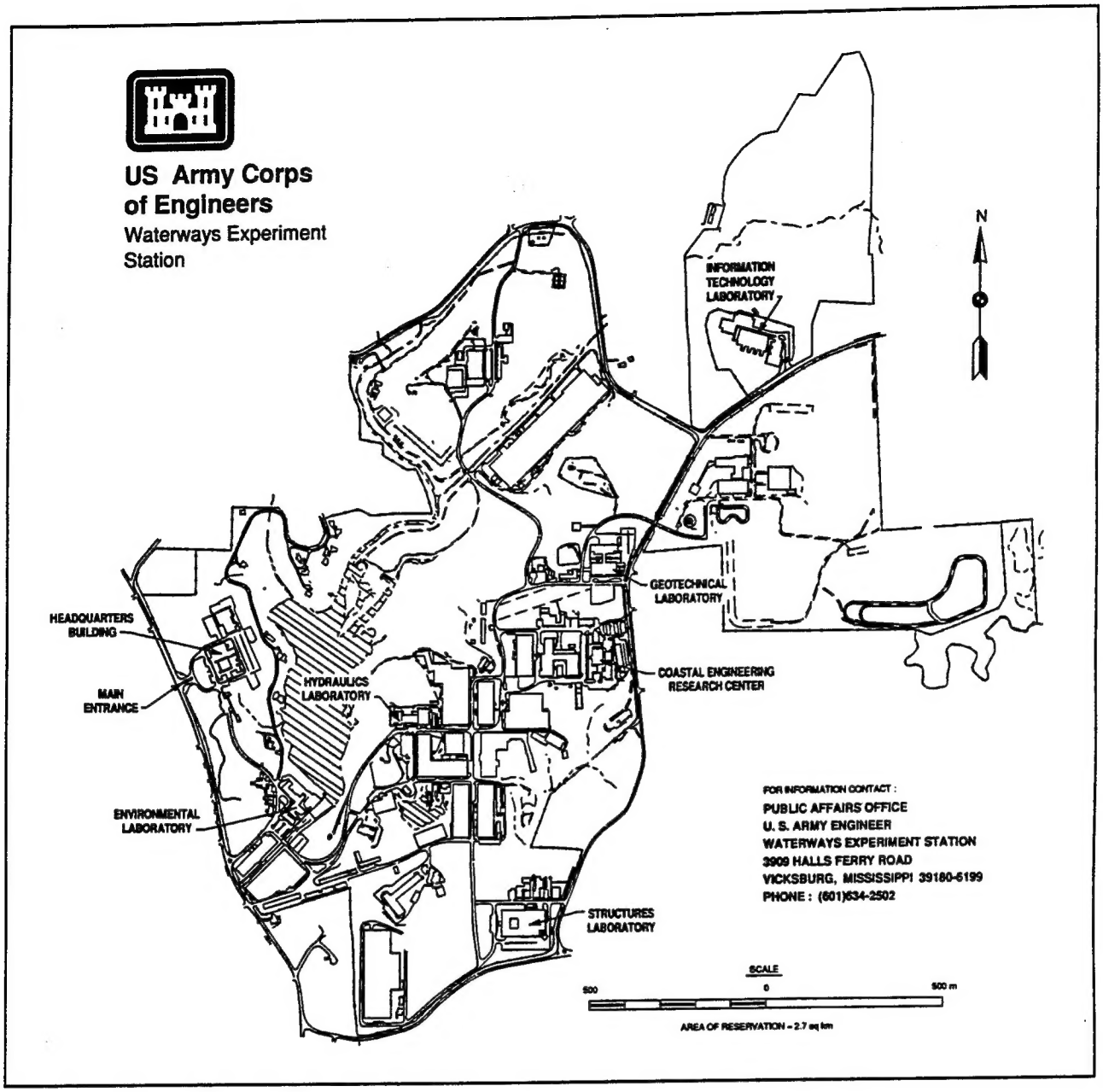

Waterways Experiment Station Cataloging-in-Publication Data

Ekler, Robert G.

Influence of geometric approximations on computational results in complex tunnel configurations / by Robert G. Ekler, Lynn W. Kennedy, Charles E. Needham ; prepared for U.S. Army Corps of Engineers ; monitored by U.S. Army Engineer Waterways Experiment Station.

58 p. : ill. ; 28 cm. -- (Contract report ; SL-95-7)

"UAST-CR-93-002"--Cover.

1. Tunnels -- Military aspects. 2. Blast effect -- Computer simulation. 3. Hydrodynamics -- Computer programs. 4. Detonation waves -- Computer simulation. I. Kennedy, Lynn W. II. Needham, Charles E. III. United States. Army. Corps of Engineers. IV. U.S. Army Engineer Waterways Experiment Station. V. Structures Laboratory (U.S. Army Engineer Waterways Experiment Station) VI. Joint U.S./ROK R&D Program for New Underground Ammunition Storage Technologies. VII. Title. VIII. Series: Contract report (U.S. Army Engineer Waterways Experiment Station) ; SL-95-7.

TA7 W34c no.SL-95-7

CONVERSION TABLE

Conversion factors for U.S. Customary to metric (SI) units of measurement

MULTIPLY → TO GET	BY	← TO GET DIVIDE
angstrom	1.000 000 X E -10	meters (m)
atmosphere (normal)	1.013 25 X E +2	kilo pascal (kPa)
bar	1.000 000 X E +2	kilo pascal (kPa)
barn	1.000 000 X E -28	meter ^{2} (m^2)
British thermal unit (thermochemical)	1.054 350 X E +3	joule (J)
calorie (thermochemical)	4.184 000	joule (J)
cal (thermochemical)/cm^2	4.184 000 X E -2	mega joule/m^2 (MJ/m^2)
curie	3.700 000 X E +1	* giga becquerel (GBq)
degree (angle)	1.745 329 X E -2	radian (rad)
degree Fahrenheit	$t_K = (t^\circ f + 459.67)/1.8$	degree kelvin (K)
electron volt	1.602 19 X E -19	joule (J)
erg	1.000 000 X E -7	joule (J)
erg/second	1.000 000 X E -7	watt (W)
foot	3.048 000 X E -1	meter (m)
foot-pound-force	1.355 818	joule (J)
gallon (U.S. liquid)	3.785 412 X E -3	meter ^{3} (m^3)
inch	2.540 000 X E -2	meter (m)
jerk	1.000 000 X E +9	joule (J)
joule/kilogram (J/kg) (radiation dose absorbed)	1.000 000	Gray (Gy)
kilotons	4.183	terajoules
kip (1000 lbf)	4.448 222 X E +3	newton (N)
kip/inch^2 (ksi)	6.894 757 X E +3	kilo pascal (kPa)
ktap	1.000 000 X E +2	newton-second/m^2 ($N\text{-}s/m^2$)
micron	1.000 000 X E -6	meter (m)
mil	2.540 000 X E -5	meter (m)
mile (international)	1.609 344 X E +3	meter (m)
ounce	2.834 952 X E -2	kilogram (kg)
pound-force (lbs avoirdupois)	4.448 222	newton (N)
pound-force inch	1.129 848 X E -1	newton-meter (N•m)
pound-force/inch	1.751 268 X E +2	newton/meter (N/m)
pound-force/foot^2	4.788 026 X E -2	kilo pascal (kPa)
pound-force/inch^2 (psi)	6.894 757	kilo pascal (kPa)
pound-mass (lbm avoirdupois)	4.535 924 X E -1	kilogram (kg)
pound-mass-foot^2 (moment of intertia)	4.214 011 X E -2	kilogram-meter^2 ($kg\cdot m^2$)
pound-mass/foot^3	1.601 846 X E +1	kilogram/meter^3 (kg/m^3)
rad (radiation dose absorbed)	1.000 000 X E -2	** Gray (Gy)
roentgen	2.579 760 X E -4	coulomb/kilogram (C/kg)
shake	1.000 000 X E -8	second (s)
slug	1.459 390 X E +1	kilogram (kg)
torr (mm HG, O°C)	1.333 22 X E -1	kilo pascal (kPa)

* The becquerel (Bq) is the SI unit of radioactivity; 1 Bq = 1 event/s.
** The Gray (GY) is the SI unit of absorbed radiation.

A more complete listing of conversions may be found in "Metric Practice Guide E 380-74," American Society for Testing and Materials.

TABLE OF CONTENTS

LIST OF ILLUSTRATIONS

LIST OF ILLUSTRATIONS (Continued)

LIST OF ILLUSTRATIONS (Concluded)

PREFACE

This study was conducted for the U.S. Army Engineer Waterways Experiment Station (WES) under contract DACA39-92-R-0063 as part of the Joint U.S./Republic of Korea R&D Study for New Underground Ammunition Storage Technologies. Technical Managers for the Joint Program were Mr. Landon K. Davis, Geomechanics and Explosion Effects Division (GEED), WES, and Dr. So-young Song, Korean Agency for Defense Development. The Program Managers were Mr. Gary Abrisz, U.S. Army Technical Center for Explosives Safety, and COL Yeon Woo Chung, Logistics Bureau, Korean Ministry of Defense.

Mr. Robert G. Eikler, S-CUBED, a Division of Maxwell Laboratories, conducted the study reported herein assisted by Dr. Lynn W. Kennedy and Mr. Charles E. Needham, coauthors of this report. The work was monitored by Mr. Charles E. Joachim, GEED, Structures Laboratory (SL), WES. Dr. Jimmy P. Balsara was Chief, GEED, and Mr. Bryant Mather was Director, SL.

At the time of preparation of this report, Director of WES was Dr. Robert W. Whalin. Commander was COL Bruce K. Howard, EN.

SECTION 1
INTRODUCTION

1.1. Purpose of the Calculation Series.

This report describes a series of calculations undertaken to compare the effects of geometric approximations/simplifications commonly made when setting up hydrodynamic code simulations of blast and flow in tunnel systems. The approximations are made to save computer resources by running the calculation in two, rather than three, dimensions. A two-dimensional calculation requires less computational time by a factor of one to two orders of magnitude. It also requires less memory to run and less storage space for the computational output. In addition, setup and analysis times are reduced. The questions to be answered by this set of calculations, which included two different two-dimensional representations as well as a three-dimensional representation, are whether the approximations provide results that are sufficiently close to those provided by calculating in three dimensions, and if so, which two-dimensional approximation is the best.

The three calculational representations are set up in the coordinate systems available in SHARC (S-Cubed Hydrodynamic Advanced Research Code), a state-of-the-art, second-order-accurate, multi-material Eulerian hydrocode. These include a two-dimensional cylindrical system, a two-dimensional Cartesian (rectangular) system, and a three-dimensional Cartesian system. Each representation includes an explosive in a detonation chamber, an input tunnel, an expansion chamber, and an output tunnel connecting to the exterior. For each chamber, cross-sectional areas and chamber volumes are the same in each configuration. Yield of the explosive source must also be conserved among the different representations. How this was accomplished is explained in detail in the next section; however, the two-dimensional representations are not unique, and some alternatives are discussed in Section 6. All of the calculations assume perfectly-reflecting, perfectly smooth tunnel wall surfaces. Hence, there are no losses to the walls. Gravitational and turbulence effects are likewise not included.

1.2. Geometric Approximations.

Three calculational configurations were specified, described as two-dimensional Cartesian, two-dimensional axisymmetric (cylindrical), and three-dimensional

Cartesian. The sketch provided by the Contract Technical Monitor to describe the configurations is included as Figure 1.

The detonation chamber was given as a cylindrical chamber, 50.20 m in length and 5.64 m in diameter. This was to be connected to the input tube shown in Figure 1 for running the various versions of the problem. Within the detonation chamber, a cylinder of TNT, 25.38 m long and with a radius of 1.41 m, was placed coaxially with its end at the remote end (away from the input tube) of the detonation chamber. The explosive was detonated at this remote end. Using a density of 1.56 gm/cm^3 for TNT with the calculated volume of the explosive cylinder, 158.52 m^3, the amount of TNT in the chamber was 247.29 metric tonnes.

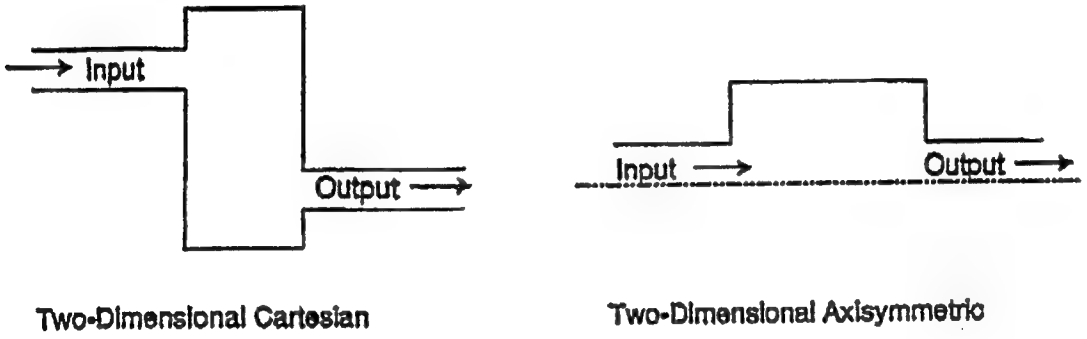

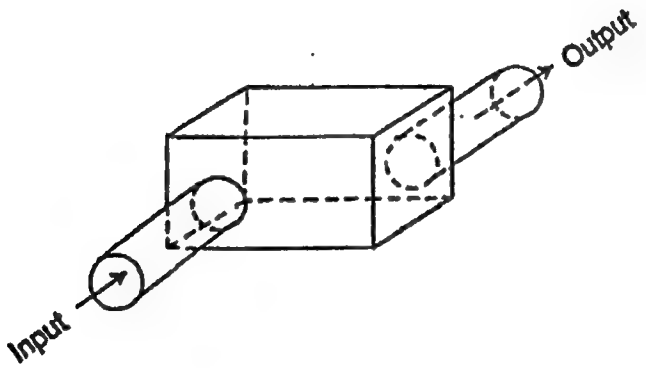

Figure 1. General configurations for expansion chamber and input and output tunnels.

Additional information provided that the input and output tunnels were 30 m in length, 8 m wide, and 6 m high. The expansion chamber was 15 m long, 70 m wide and 8 m high. The lateral offset between the input and output in the Cartesian configurations was to be set at 58 m.

1.2.1. Cylindrical Configuration.

This configuration was the easiest to set up and hence was done first. The explosive chamber and explosive within it were provided as cylinders and therefore could be left as specified above. The lengths of the input and output tunnels were retained at 30 m, and the cross-sectional areas were preserved at 8 m x 6 m = 48 m^2. This resulted in a radius for the equivalent cylindrical input and output tunnels of 3.91 m. The expansion chamber was given a cylindrical equivalent in the same manner, retaining the length of 15 m and calculating an equivalent radius to preserve the cross-sectional area. The area was 70 m x 8 m = 560 m^2, thus the cylindrical equivalent radius is 13.35 m. The final configuration used for the cylindrical calculation is given in Figure 2.

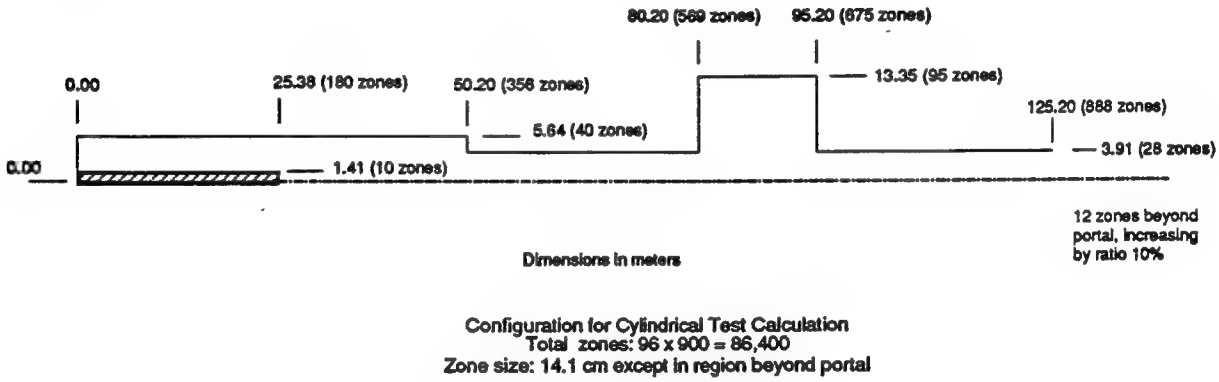

Figure 2. Configuration and zoning used for cylindrical calculation.

1.2.2. Two-Dimensional Cartesian Configuration.

For a two-dimensional Cartesian calculation, it is necessary to choose a "unit height," or dimension normal to the two dimensions of the calculational mesh, which is the same for every part of the calculation. Because the input and output tunnels are 6 m high, we chose 6 m as the unit height. The dimensions of these two tunnels thus remained the same, and those of the detonation and expansion chambers were adjusted to give them equivalent cross-sectional area using the 6-m unit height. The lateral dimension of the explosive was adjusted in the same way to retain the total yield.

The cylindrical explosive chamber has a radius of 5.64 m, making its cross-sectional area 99.93 m^2. Therefore, for a 6-m unit height in rectangular coordinates, its width must be 99.93 m^2/6 m = 16.66 m. The length of the chamber is retained at 50.20 m. Similarly, the expansion chamber has a cross-sectional area of 560 m^2, as given with the 8-m height. To retain the length and volume of this chamber with the 6-m height, we have to in-

crease its width from 70 m to 93.33 m. The lateral offset between the input and output tunnels was retained at the given 58 m, so the additional width resulted in larger alcoves at the sides of the expansion chamber.

The dimensions of the explosive had also to be adjusted so that the proper explosive yield would be contained in the Cartesian problem. The volume of TNT, as calculated above, is 158.52 m^3. Retaining its length at 25.38 m so that the detonation will occur at the proper rate, and using the 6-m unit height, the width of the explosive slab is 1.04 m. All of the dimensions used in this configuration are shown in Figure 3. Note that this is a plan view, so that discussions of width or lateral dimension are shown vertically on the paper, while length is shown horizontally. The unit height, a constant 6 m, is normal to the plane of the paper.

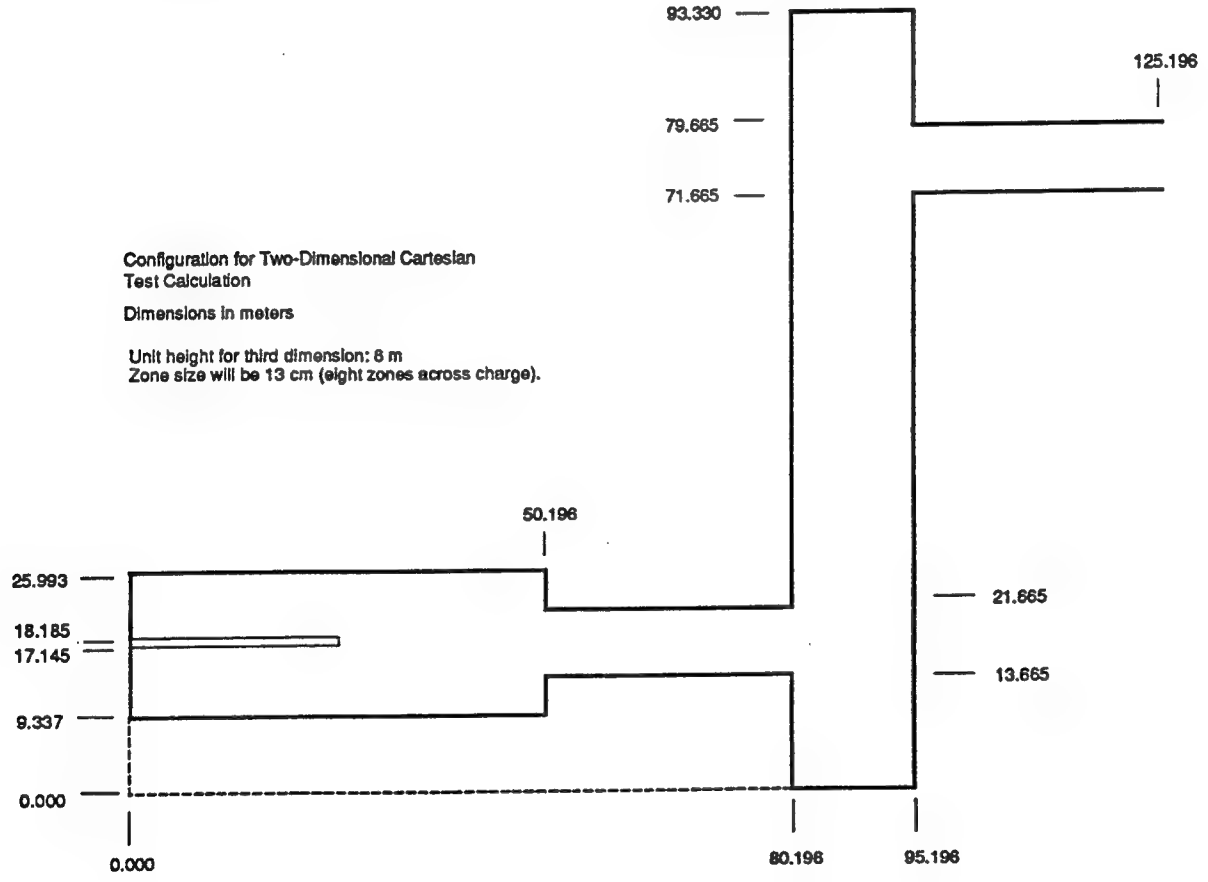

Figure 3. Configuration for two-dimensional Cartesian problem set-up.

1.2.3. Three-Dimensional Configuration (Cartesian).

The three-dimensional problem was more difficult than the others because of the complexities of visualizing and displaying the three-dimensional representation. Because

everything could be represented exactly as it was provided, this phase of the setup was straightforward. The detonation chamber, input tunnel, and explosive were all cylindrical and, in fact, the first phase of the problem utilized the same calculation that had been generated for the cylindrical representation. We did not begin the three-dimensional part until the explosive was completely detonated and the shock wave had progressed through the input tube and was beginning to move into the expansion chamber. At this point the three-dimensional configuration illustrated in Figure 4 was set up. Because the three-dimensional code allows cylindrical packages in the Cartesian mesh, representing them as closely as possible following cell boundaries, no modifications to the chamber shapes beyond those defined by the "stair-step" cell boundaries were required. Figure 5 is an isometric projection of the information provided in Figure 4, and may be helpful in visualizing the configuration.

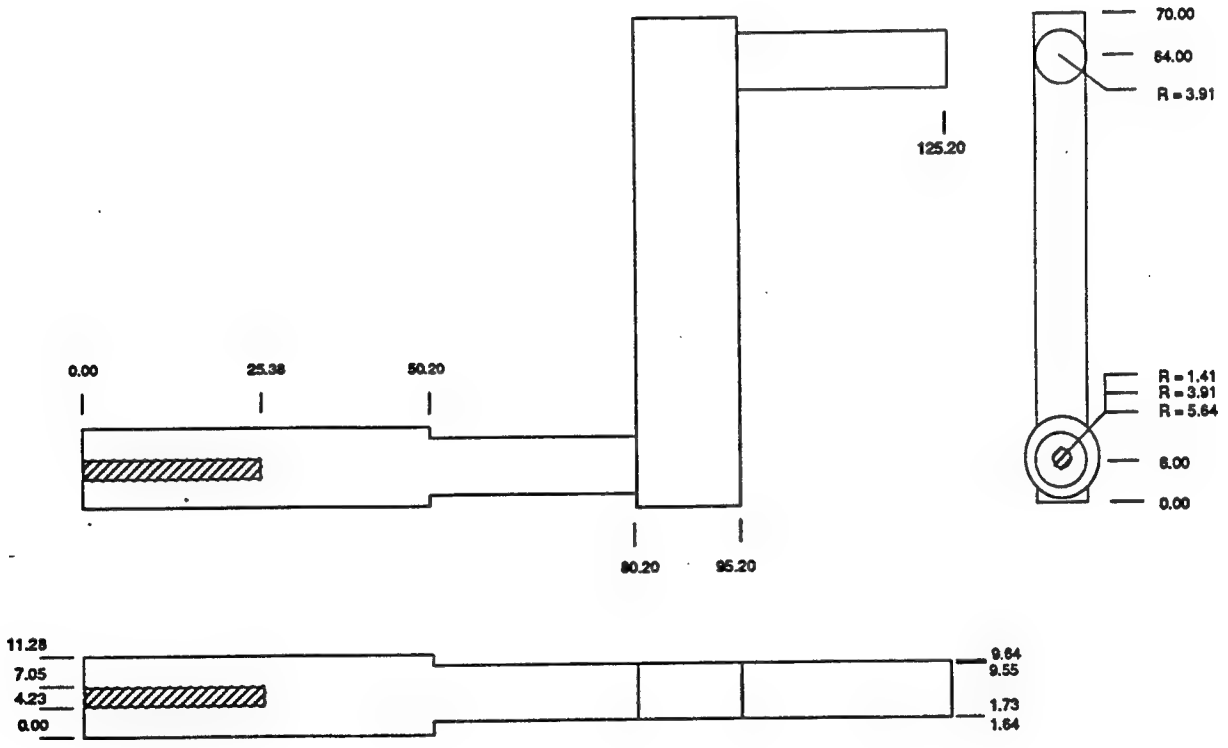

Figure 4. Configuration drawing for three-dimensional Cartesian problem set-up.

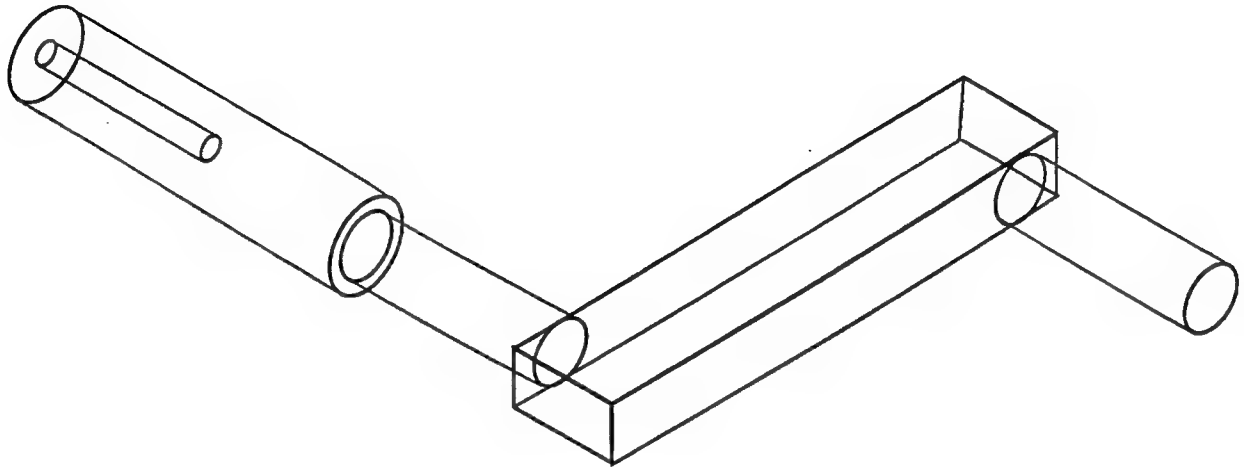

Figure 5. Orthogonal drawing for three-dimensional configuration.

SECTION 2
CALCULATION SETUP

2.1. Cylindrical Configuration.

The cylindrical calculation is radially symmetric about a vertical* axis and is constructed uniformly with 14.1 cm zones in both coordinate directions. For the charge detonation, or first phase, of this calculation, the fluid region extends horizontally to a radius of 5.64 m. Two additional zones of perfectly reflecting solid are placed to the right, extending the computational domain to 5.922 m. Vertically, the domain extends to 50.196 m. A cylindrical region with a radius of 1.41 m and length of 25.38 m is specified as TNT. An explosive mass of 247 metric tonnes is generated which contains 6.56×10^{17} ergs of ambient internal energy. The detonation of this cylinder of TNT is initiated with a hemispherical region of high-energy gaseous detonation products. This region is 19 cm in radius and is located at the base of the TNT on its centerline. The initialization hemisphere radius is assigned to correspond to initialization time at 29 microseconds, assuming initiation at the center at time 0 and a detonation velocity of 6.5×10^5 cm/s. After 29 microseconds, detonation proceeds normally through the TNT according to well-established burn routines in the hydrocode. Figure 6 illustrates the configuration of the initial cylindrical detonation calculation.

The data representing the initial conditions as described was processed by SHARC, using second-order alternating direction remapping, a multi-material equation of state, and a high-explosive burn routine. The high-explosive burn was complete at 4 milliseconds. At 8 milliseconds, the shock front was close enough to the top boundary of the computational domain to necessitate remapping the calculation to a larger domain.

The larger domain consists of uniform 14.1 cm zones in the radial direction to a distance 13.82 m. In the vertical direction, the zones are 14.1 cm uniformly to a height of 125.20 m and expand geometrically beyond that point by 10% from one zone to the next, to a final height of 128.20 m.

---

* The "vertical" and "horizontal" designations here and in Figures 6 and 7 are reversed from those shown in Figures 1 and 2. The latter were drawn to correspond to physical reality; the former are as displayed by the hydrocode. Because there is no treatment of gravity in these calculations, the results are not affected.

The fluid region is extended into three additional chambers. The first extends the fluid region 30.03 m to a height of 80.22 m. This extension is constricted to a width of 3.948 m in order to provide a chamber of comparable cross-section and length to the prescribed input tube. The second extends the fluid region 14.94 m to a height of 95.17 m. This chamber expands to a width of 13.395 m in order to provide the appropriate volume for the expansion chamber.

The final (output) chamber replicates the input chamber using the same length and width. It extends the fluid region to a height of 125.208 m. Beyond this position are expanded zones and transmissive boundaries in either direction. The shock may expand without restriction in this region. Figure 7 illustrates the configuration for the remap of the cylindrical calculation.

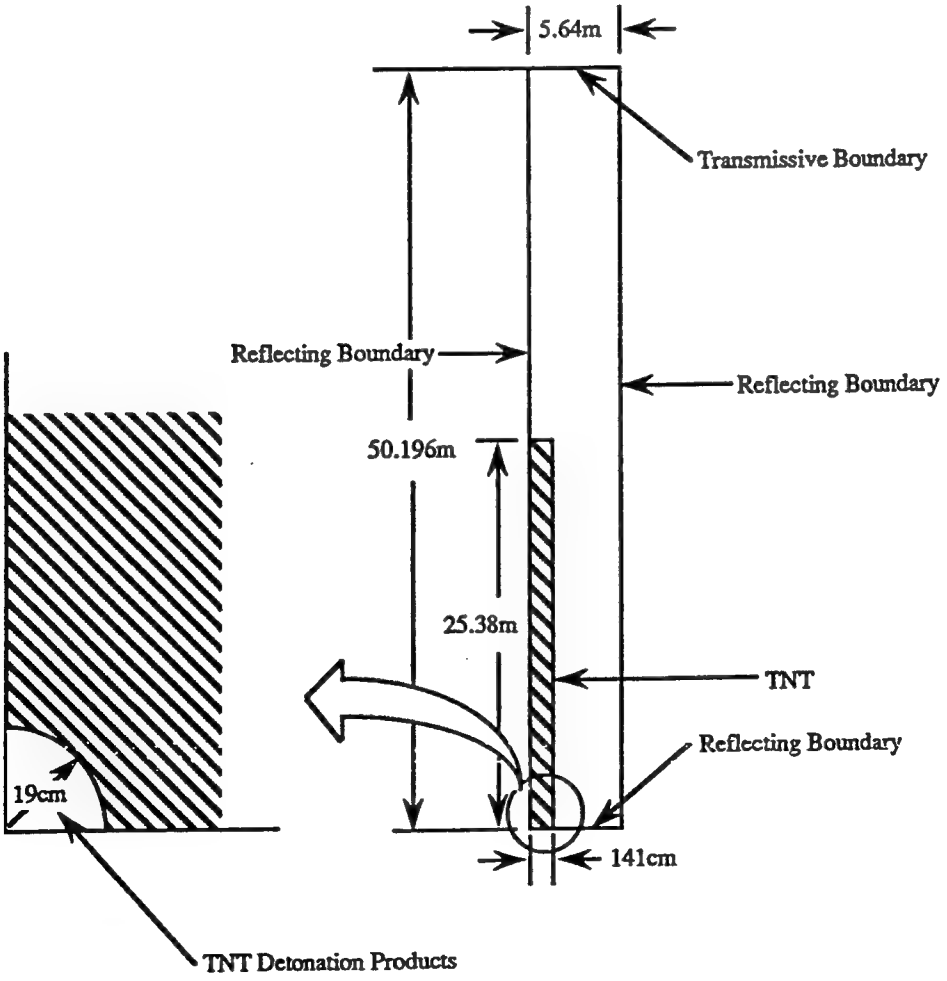

Figure 6. Configuration for initial detonation calculation in cylindrical symmetry.

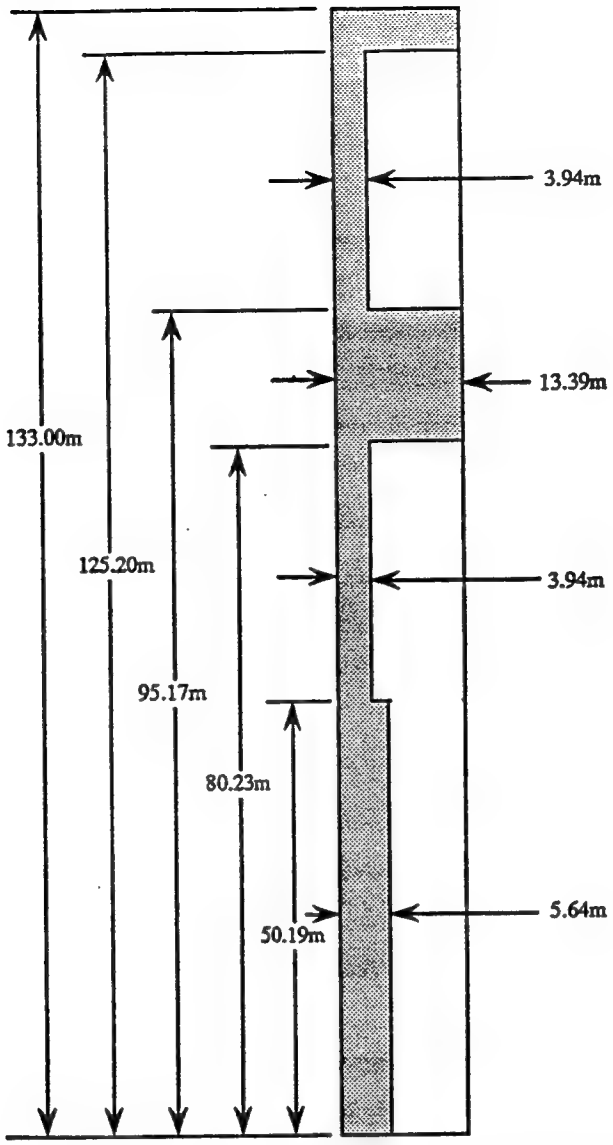

Figure 7. Configuration for remap of cylindrical calculation.

2.2. Two-Dimensional Cartesian

The two-dimensional Cartesian calculation consists initially of a domain extending horizontally to 95.42 m and vertically* to 35.36 m. The fluid region consists of two horizontally-oriented and one vertically-oriented chambers. Each of the chambers and passageways is assigned a unit depth of 6 m.

The chamber in which the detonation is initiated is 16.64 m wide and 50.18 m long. It is oriented horizontally with its centerline vertically offset from the bottom of the mesh by

* Because this is a plan view, "vertical" means lateral across the width of the expansion chamber, just as in Figure 3.

17.68 m. Specified within this chamber, along its centerline, is a region of TNT 1.04 m wide and 25.35 m in length. This rectangle when multiplied by the 6-m unit depth, contains a volume corresponding to 247 metric tonnes of TNT. The calculation of detonation within this region is initiated with a semi-circular region of high energy, gaseous detonation product 39 cm in diameter. The calculation is assigned an initial time of 59 microseconds to correspond to this diameter.

Adjacent to the detonation chamber is a constrictive passageway (the input chamber) 30.0 m long and 8.06 m in width. One additional, vertically-oriented, rectangular chamber is located to the right of the passageway. It extends the fluid region 14.95 m to a horizontal distance of 95.16 m from the origin, and represents part of the expansion chamber. Figure 8 illustrates the configuration of the initial Cartesian detonation calculation. The zone size for this part of the calculation is 13 cm in both coordinate directions.

The data representing the initial condition as described was processed by SHARC, as in the previous case. The high explosive burn was complete at approximately 4 milliseconds. At 18 milliseconds, the shock front was close enough to the top boundary of the computational domain to necessitate remapping to a larger domain.

The larger domain includes an extension of the vertically-oriented expansion chamber to 93.34 m. Additionally, a horizontally-oriented output chamber 30.0 m by 8.0 m is located adjacent to the expansion chamber. Its centerline is vertically offset 75.66 m. The zones to the left of the entrance to the expansion chamber expand geometrically with a 10% expansion ratio to reduce the size of the computational files and processing time. Figure 9 illustrates the configuration of the final remap of the two-dimensional Cartesian calculation.

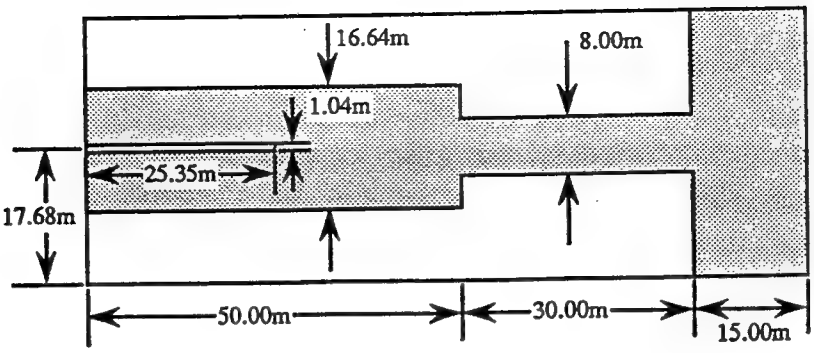

Figure 8. Configuration for initial detonation calculation in Cartesian coordinates.

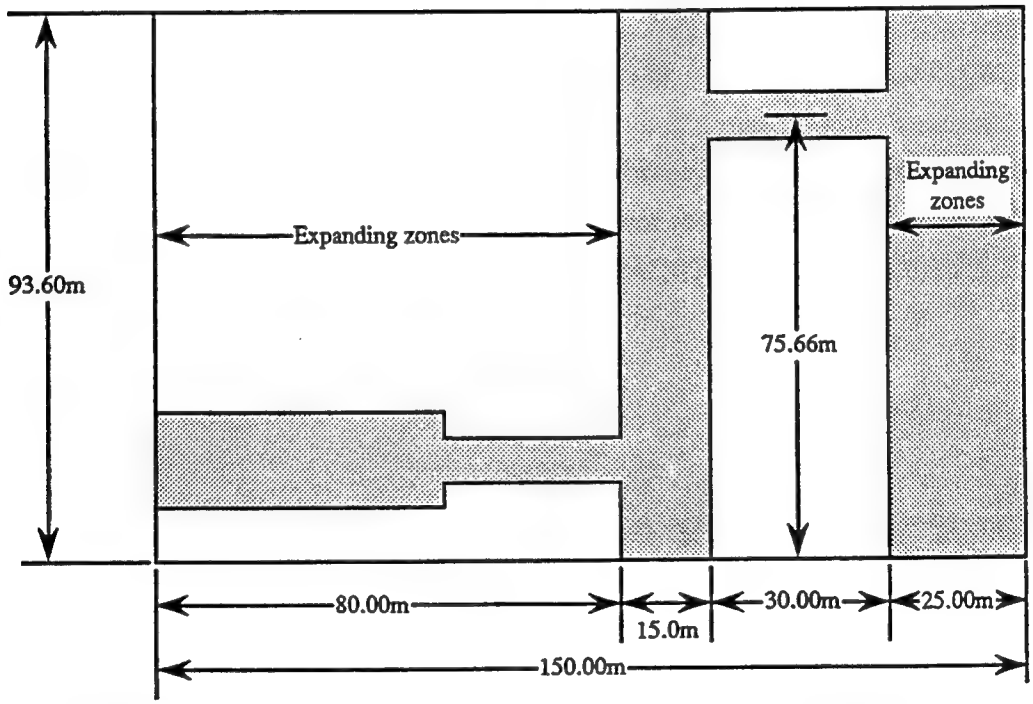

Figure 9. Configuration for remap of Cartesian calculation.

2.3. Three-Dimensional Cartesian Calculation.

The three-dimensional Cartesian calculation consists initially of two adjacent half-cylinders and a rectangular prism in a domain extending 95.00 m horizontally and 35.36 m vertically. The cylinders and rectangular prism are halved in order to exploit symmetry

of the configuration above and below a horizontal mid-plane. The half-cylinders were initialized with the hydrodynamic parameters from the two-dimensional cylindrical calculation at 14 milliseconds. The two-dimensional cylindrical data is extrapolated into the three-dimensional coordinate system by using a rotation transformation algorithm. The horizontal (x-coordinate) sizes of the zones are geometrically expanded from the entrance of the rectangular prism leftward to the origin using a 10% expansion ratio. Zones within the rectangular prism are 15 cm in the x-coordinate dimension. In the vertical (z-coordinate) and page-normal (y-coordinate) the zone size is 14.1 cm. At 23 milliseconds, the shock front was close enough to the top boundary of the computational domain to necessitate remapping the calculation to a larger domain.

The next larger domain was extended vertically to 60.0 m. The zone sizes remained unchanged. At 34 milliseconds, the shock front position necessitated remap to a still larger domain. The next remap extended the domain both horizontally and vertically. Horizontal (x-coordinate) and vertical (y-coordinate) zone sizes were doubled, to 30 cm. A cylindrical output chamber was placed adjacent to the rectangular prism representing the expansion chamber at a vertical offset of 64.0 m. An unrestricted expansion region was included beyond the output chamber. The horizontal zones within both these regions expanded geometrically at a 10% ratio. Figure 10 illustrates the final configuration of the three-dimensional Cartesian configuration.

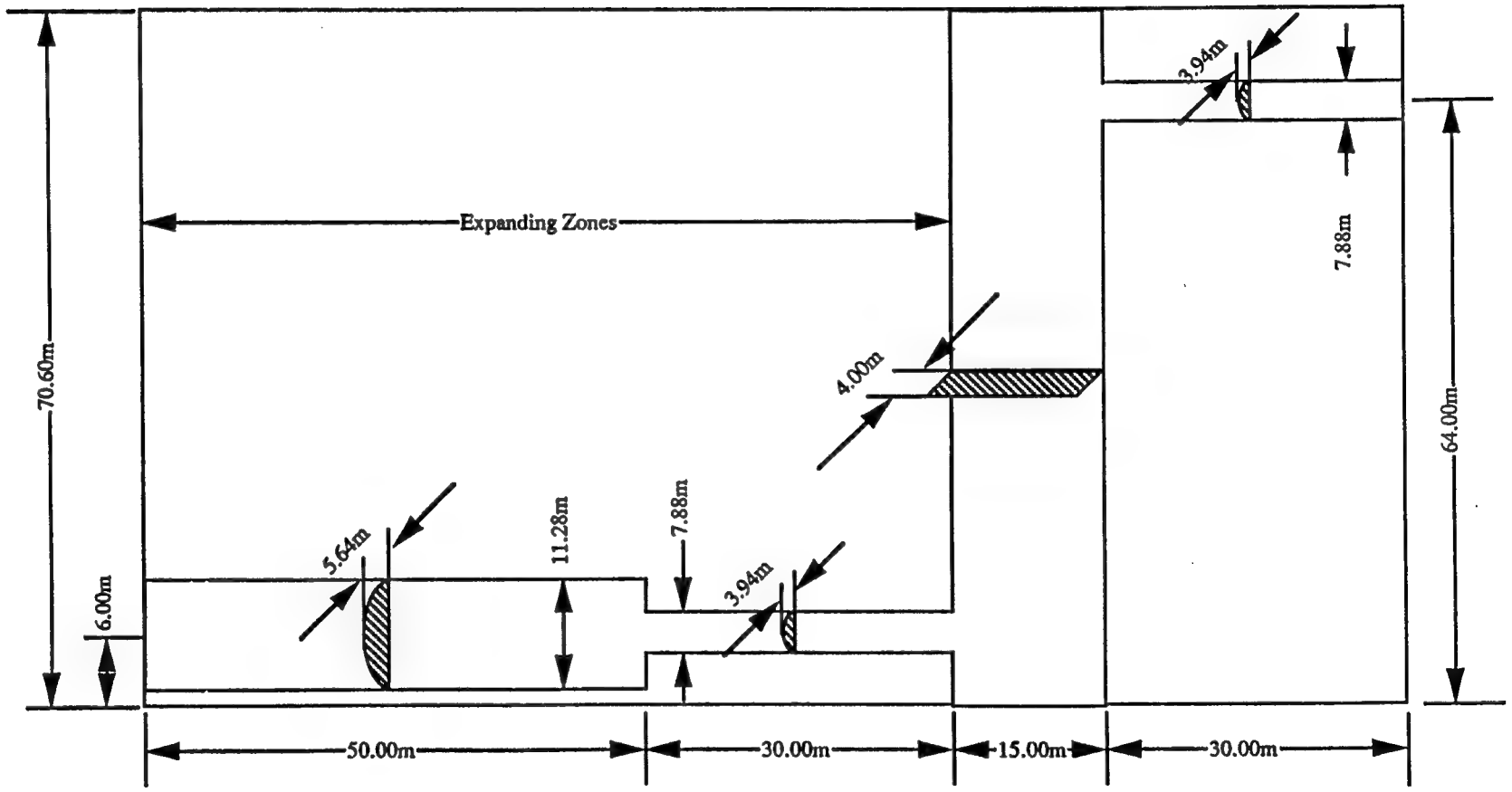

Figure 10. Configuration for final remap of three-dimensional Cartesian calculation.

SECTION 3
CALCULATIONAL RESULTS

Figures 11 and 12 are pressure contour plots for the two-dimensional cylindrical and Cartesian configurations at 2 milliseconds. A separate plot for the three-dimensional configuration has not been included, because it is identical to the cylindrical configuration at this early time. At this time, the shock front is at about the same position for each case. The maximum pressure is somewhat lower (about 20%) in the Cartesian chamber, probably because there are more computational zones across the cylindrical explosive, and hence the pressure is not relieved as quickly as in the Cartesian case. The cylindrical result is probably a better approximation of reality during the explosive detonation. In both cases, reflected shocks are proceeding inward from the chamber walls.

Figures 13 and 14 are pressure contour plots at 8 milliseconds. These plots show that the 2-D Cartesian shock front has advanced 4 m beyond the position of the cylindrical shock. The Cartesian shock front is already reflecting off the end wall of the detonation chamber. The shock structures differ significantly because of the geometry. In the cylindrical configuration, a Mach stem is evident on the axis, whereas no such structure shows in the Cartesian contour plot. The maximum pressure is about a factor of 2.5 stronger in the cylindrical chamber. These effects are almost surely a result of cylindrical convergence on the axis of waves reflected at the chamber walls. The Cartesian configuration does not generate geometric convergence.

Figures 15, 16, and 17 are pressure contour plots at 16 milliseconds. Because the 2-D cylindrical configuration was mapped into the 3-D mesh at 14 milliseconds, the 3-D Cartesian is a distinct calculation at 16 milliseconds and is included for comparison. The contours shown are on the horizontal reflecting plane at the center of the configuration. At 16 milliseconds, the shock wave is entering the expansion chamber in each case. The 2-D Cartesian case has an unrealistically long alcove at the end of the expansion chamber (bottom right of the plot), made necessary by the scheme used to maintain the same expansion chamber volume in all three cases. This means that the end wall reflection occurs much later in this case than in the 3-D case. Note that, at this time, the maximum pressure occurs in the 2-D Cartesian case.

Figures 18, 19, and 20 are pressure contour plots at similar, but not exactly the same, times. The Cartesian plots are taken at 26 ms for the 3-D and at 25 milliseconds for the 2-D. The shock structures are similar at these times. For the Cartesian cases, the shock

front is a diagonal across the expansion chamber, arriving earlier at a position close to the far wall than at a corresponding position on the near wall. The cylindrical case cannot be easily compared to the others at these times, because the shock, having a much shorter distance to travel through the expansion chamber, has gone on into the output tube and is near the tunnel portal.

Figures 21 and 22 are pressure contour plots showing shock front development at 36 milliseconds. The 2-D Cartesian case has a shock front a bit further into the output chamber than does the 3-D case. This is because the 3-D expansion chamber is taller (8 m as opposed to the 6-m unit height of the 2-D configuration), and hence the shock front has more room in which to expand. This will allow the shock-front pressure to decay more rapidly and hence the front will not travel as fast. This volume effect is eventually equalized, but not until the wave has completely filled the alcove at the end of the chamber. We do not show a cylindrical contour at this time because for this case, the shock has exited the output tunnel.

The next group of figures consists of comparisons of overpressure records obtained from the three calculations at corresponding points in the interior and at the portal. Figure 23 provides a comparison of the overpressure signal at the detonation chamber exit. Only the 2-D cylindrical and the 2-D Cartesian are compared because the 3-D Cartesian is identical to the 2-D cylindrical at this location. The signal beyond the initial shock arrival peaks is roughly comparable with respect to amplitude and general waveform. Differences in timing and amplitude of the various peaks occur because of differences in the explosive configuration and in the distances and orientations of various reflecting surfaces relative to the measurement location.

Figure 24 compares overpressure waveforms at locations in the center of the input tube. As expected, the arrival times are nearly identical. The peak overpressure is somewhat lower in the Cartesian case, but the generation of impulse, as shown in Figure 25, is approximately equivalent. Similar results at the input tube/expansion chamber junction are shown in Figures 26 and 27.

Figure 28 compares the signals obtained near the center of the expansion chamber. The three-dimensional result is included for this and the following comparisons because at this location, the record is different from that of the cylindrical calculation. The cylindrical record exhibits an earlier arrival time because the path over which the shock wave travels is shorter. It is also greater in amplitude. The Cartesian cases appear to have

similar magnitudes for the initial 5 milliseconds after shock arrival. The late-time signal is stronger in the 3-D case, possibly because of the larger alcove volume of the expansion chamber in the 2-D configuration.

Figure 29 compares signals from the center of the output tube. Again, the cylindrical signal arrives much earlier and has higher peaks. The Cartesian cases are in closer agreement, although there are noticeable differences in waveform details. The same may be observed at the exterior opening of the output tube, as shown in Figure 30.

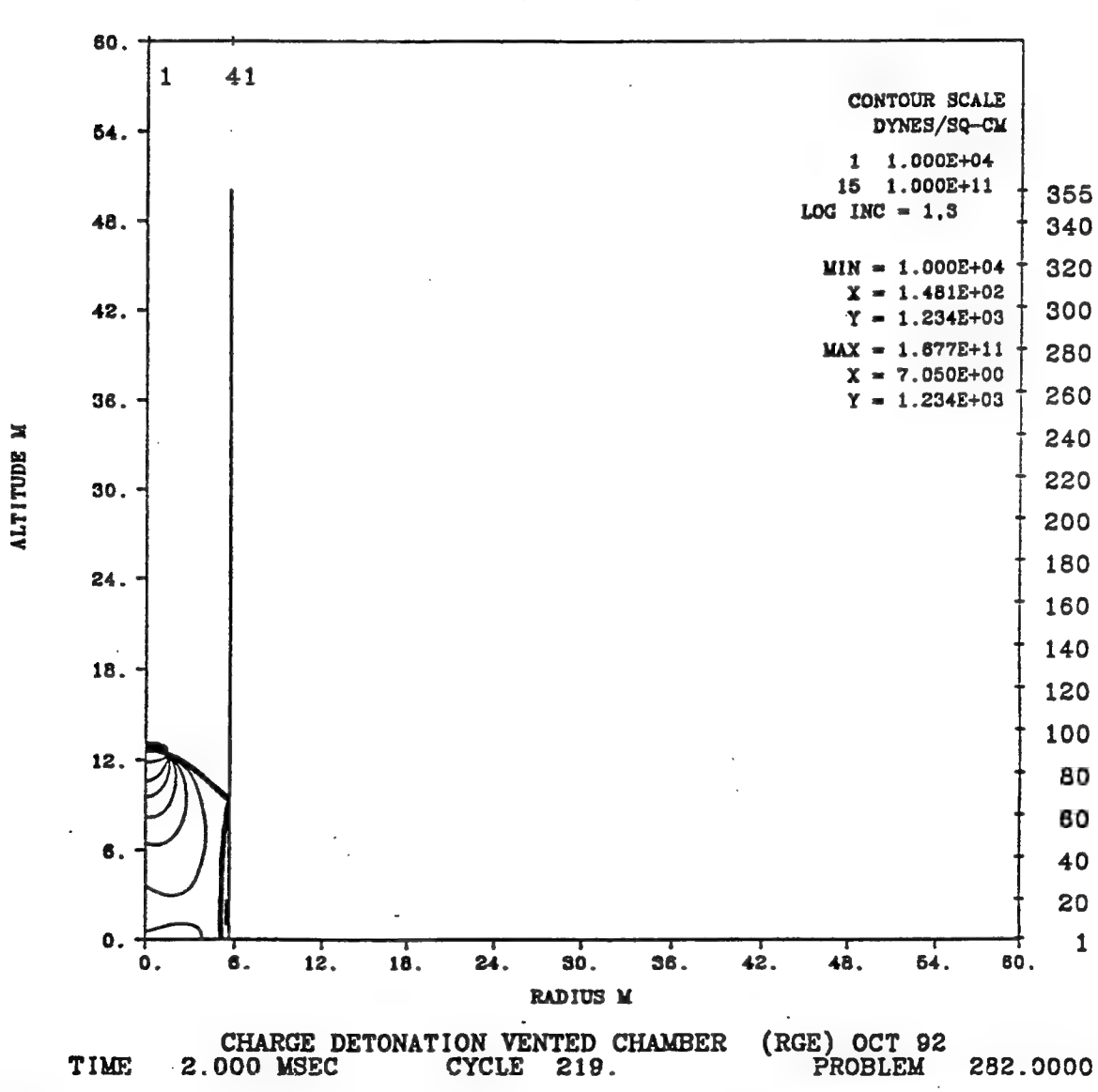

Figure 11. Pressure contour plot for two-dimensional cylindrical detonation calculation at 2 ms.

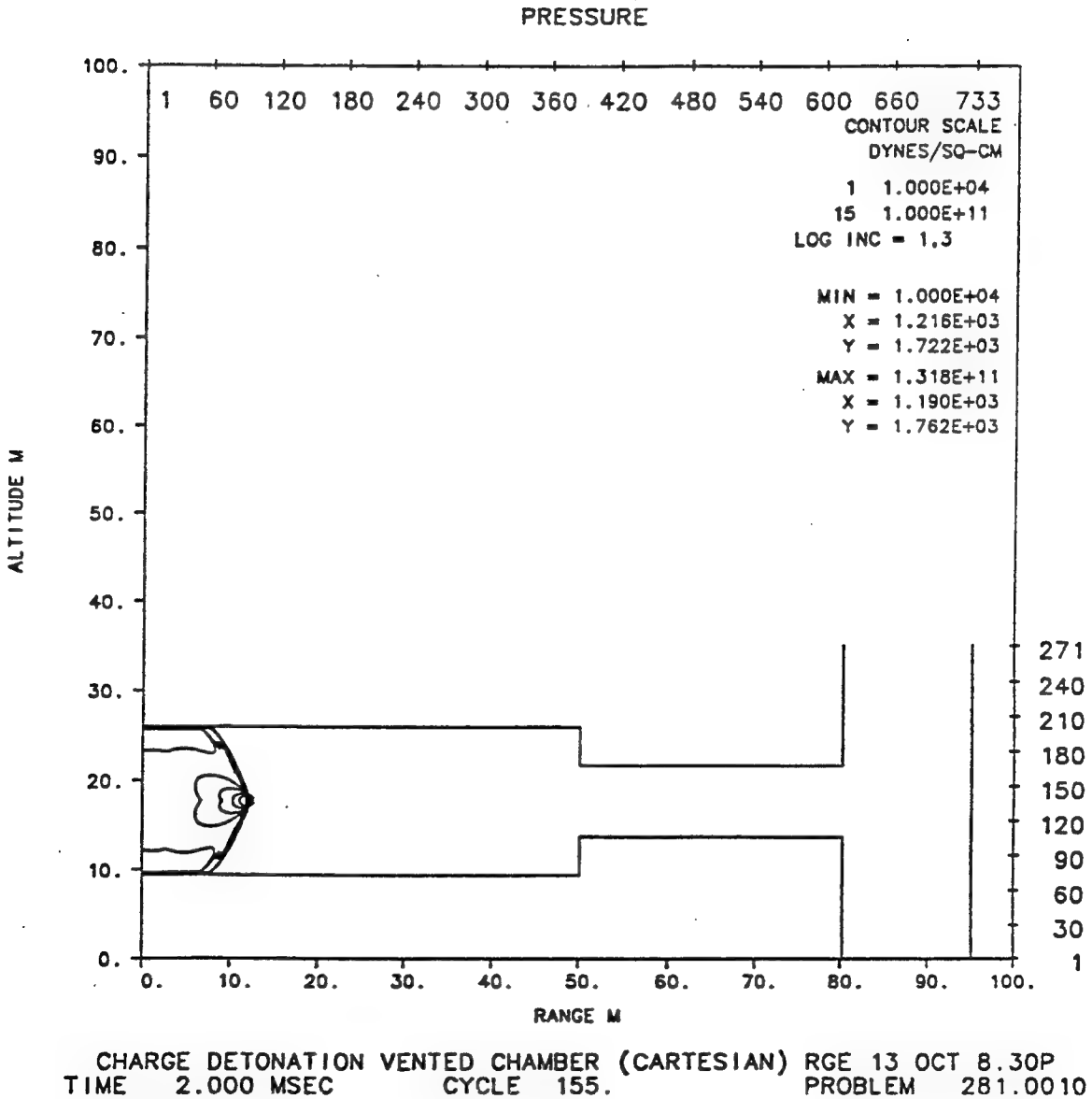

Figure 12. Pressure contour plot for two-dimensional Cartesian detonation calculation at 2 ms.

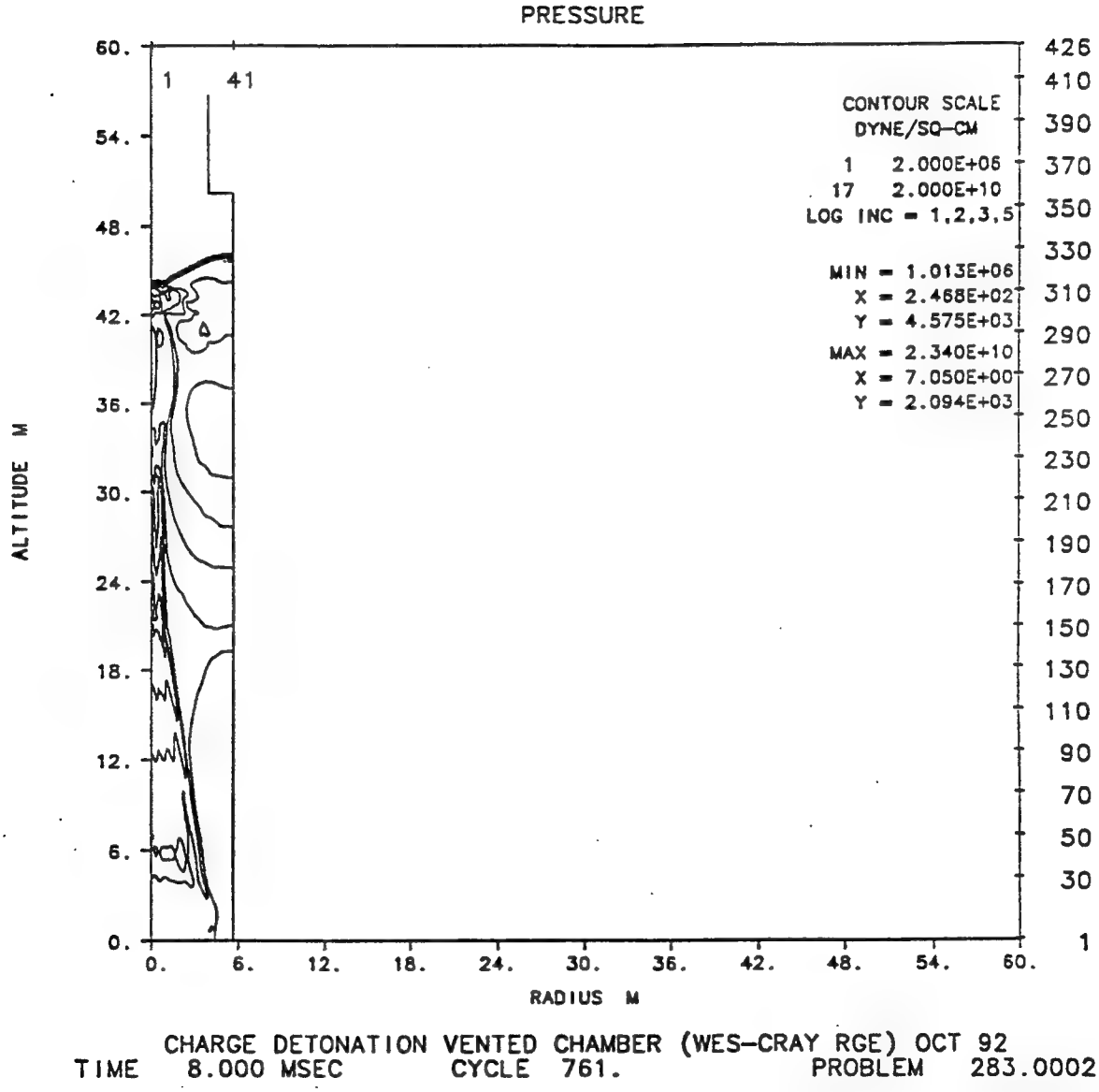

Figure 13. Pressure contour plot for two-dimensional cylindrical calculation at 8 ms.

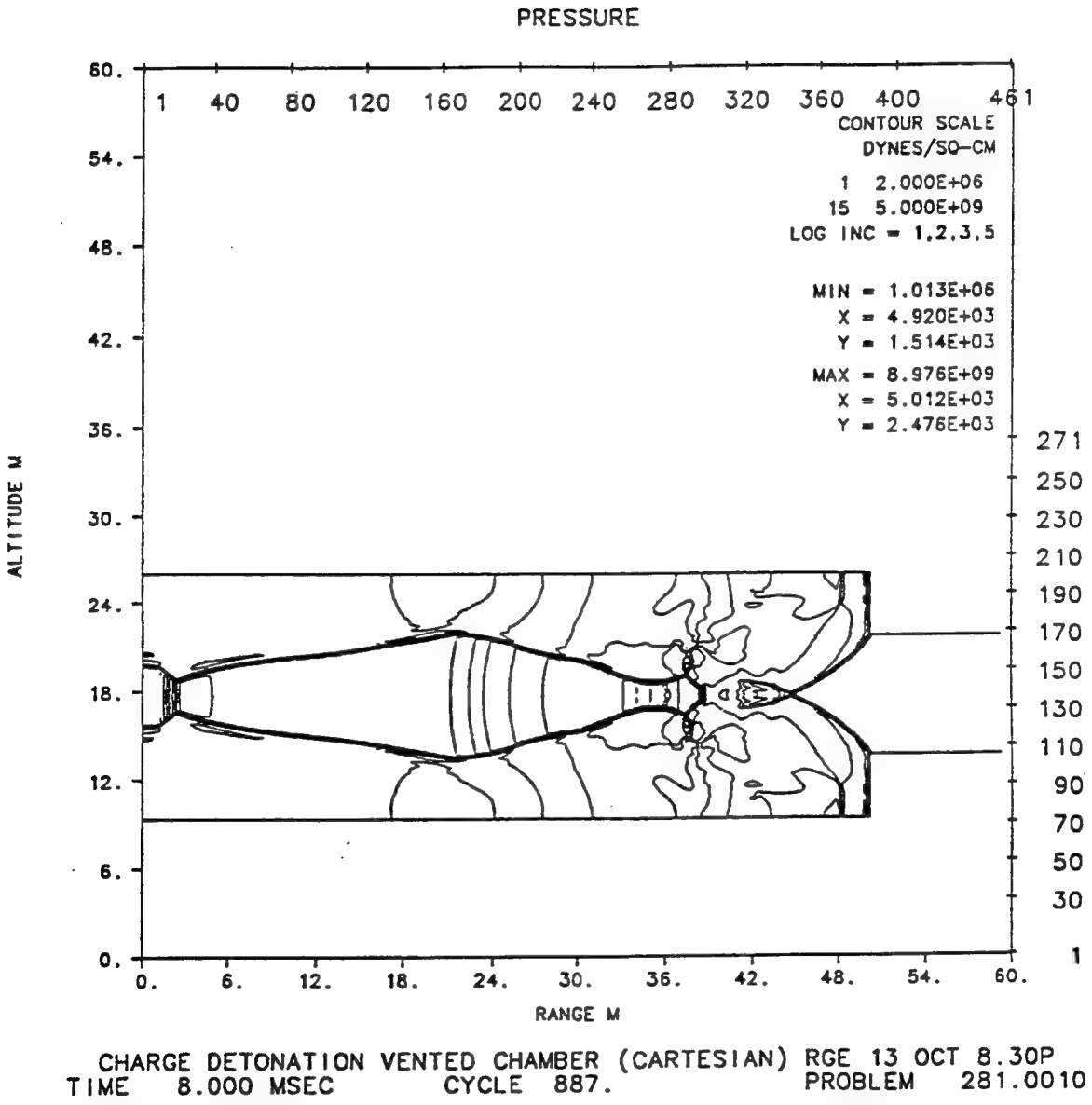

Figure 14. Pressure contour plot for two-dimensional Cartesian calculation at 8 ms.

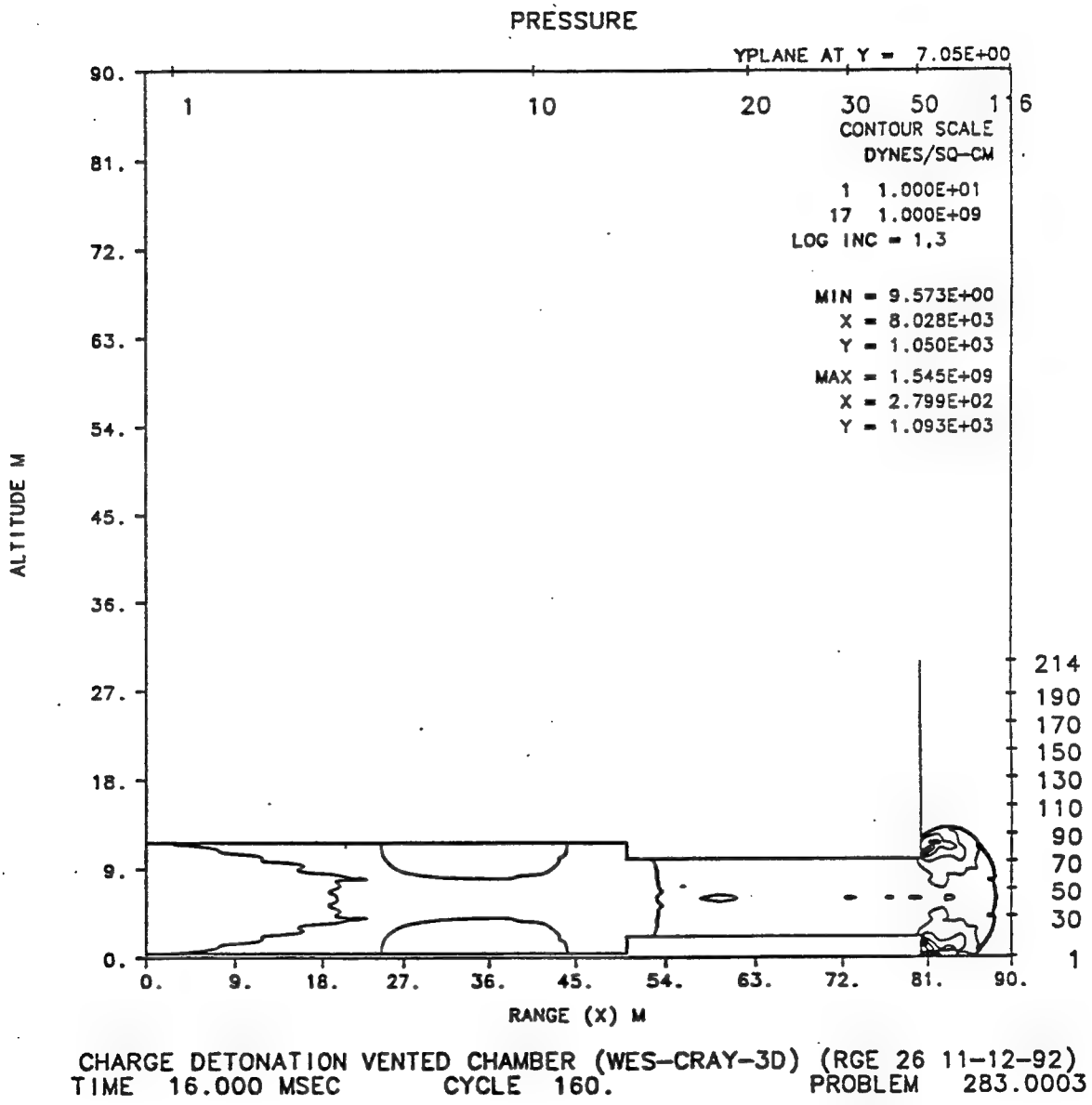

Figure 15. Pressure contour plot for three-dimensional Cartesian calculation at 16 ms.

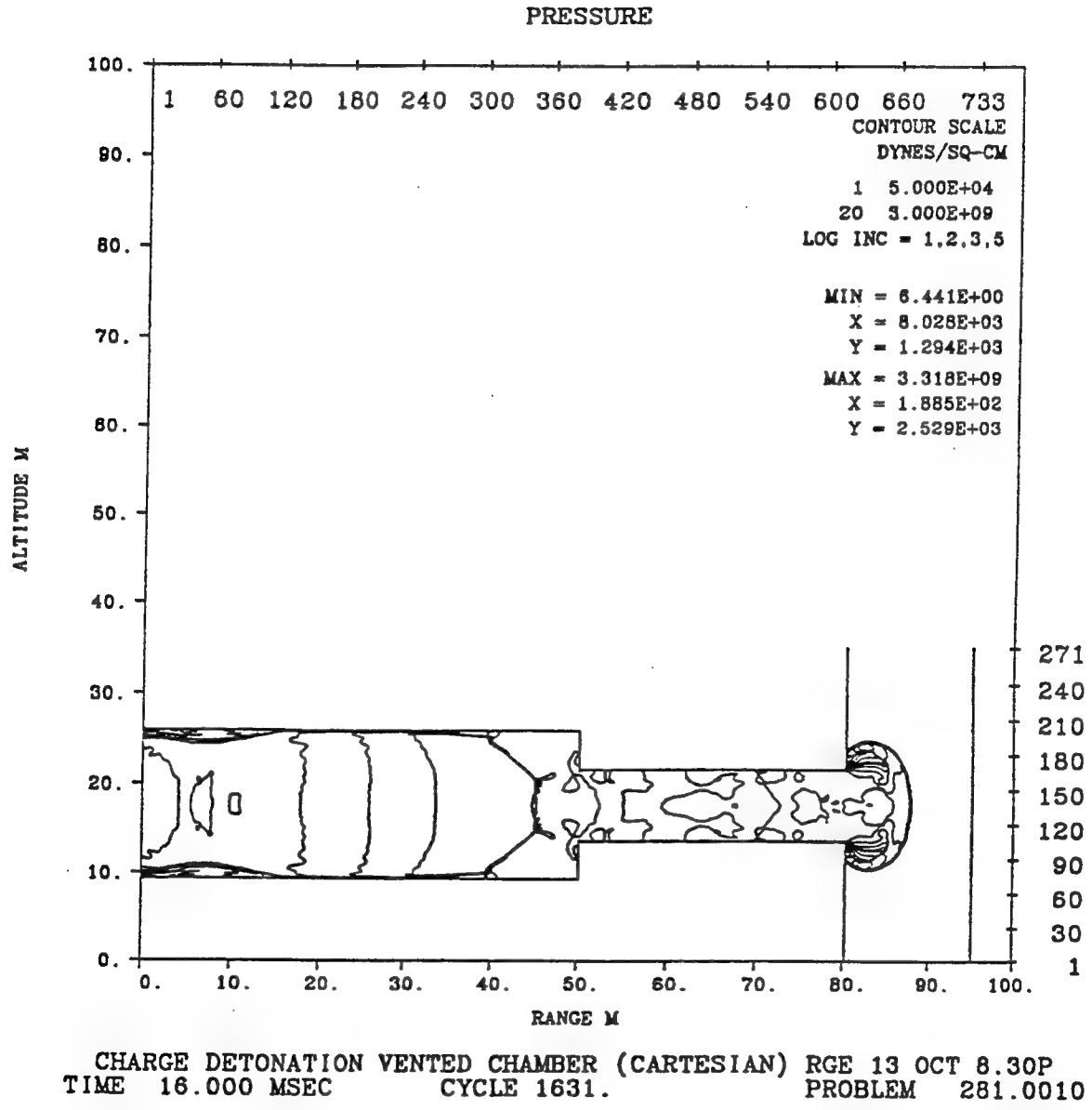

Figure 16. Pressure contour plot for two-dimensional Cartesian calculation at 15 ms.

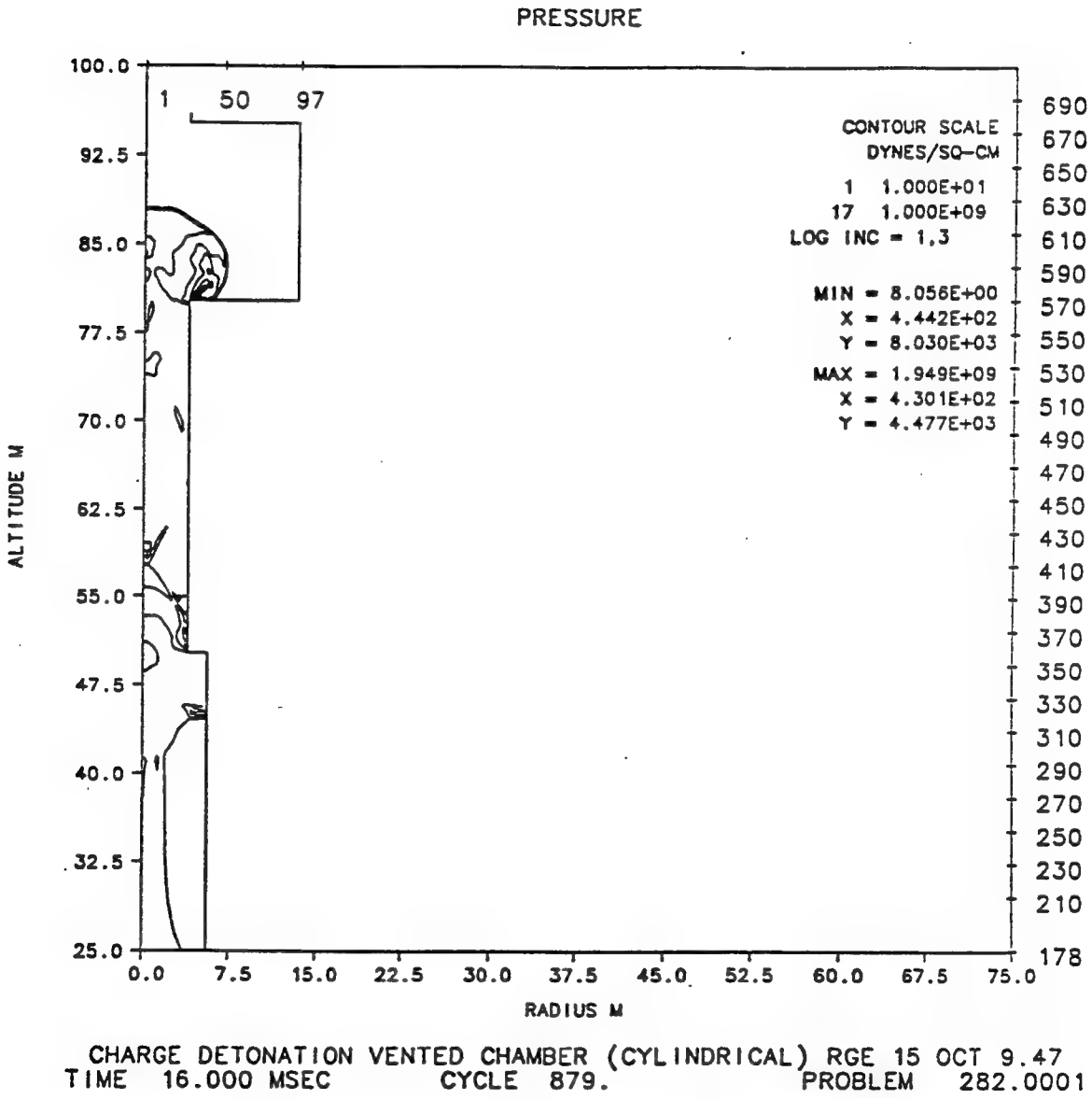

Figure 17. Pressure contour plot for two-dimensional cylindrical calculation at 16 ms.

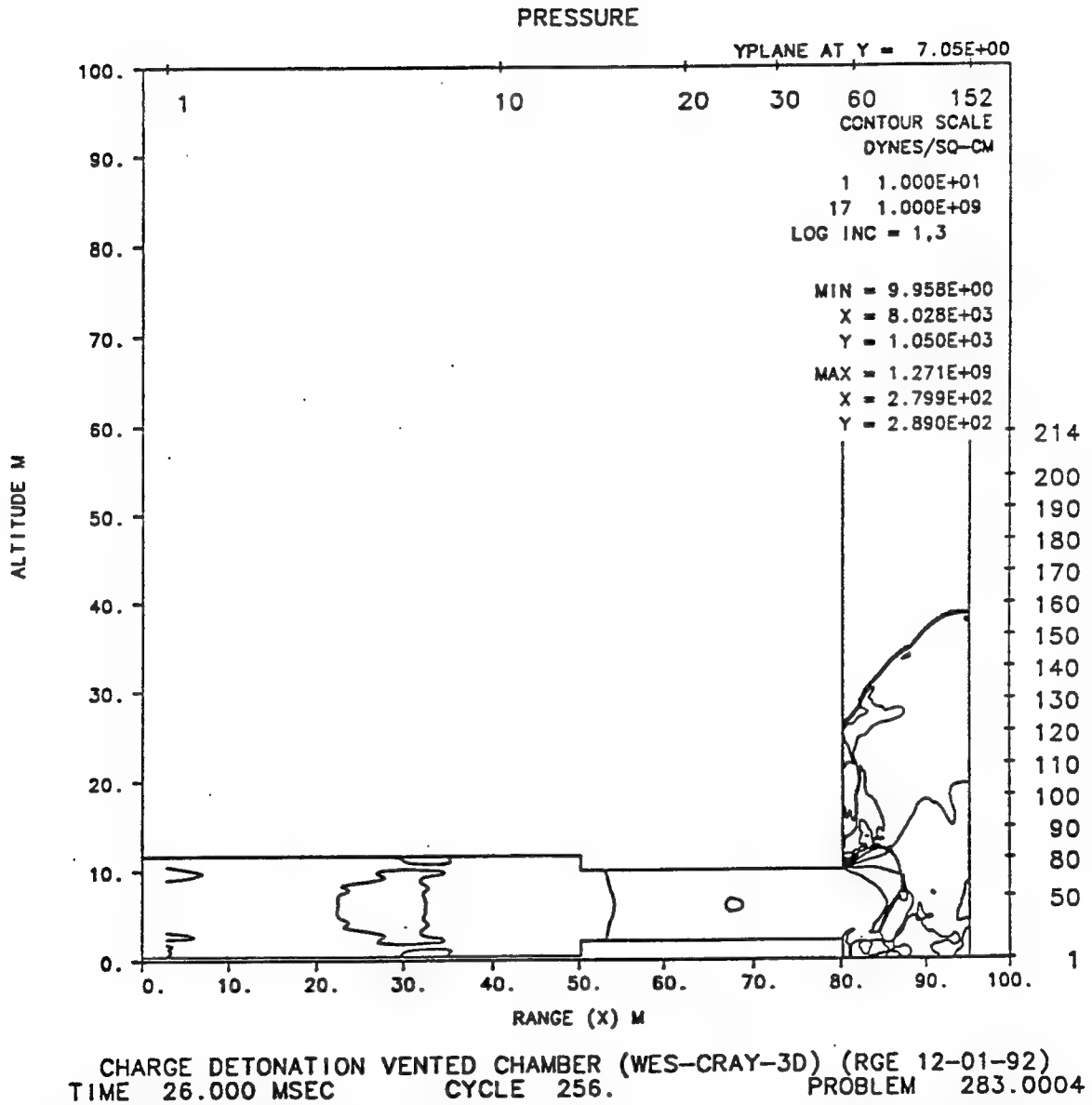

Figure 18. Pressure contour plot for three-dimensional Cartesian calculation at 26 ms.

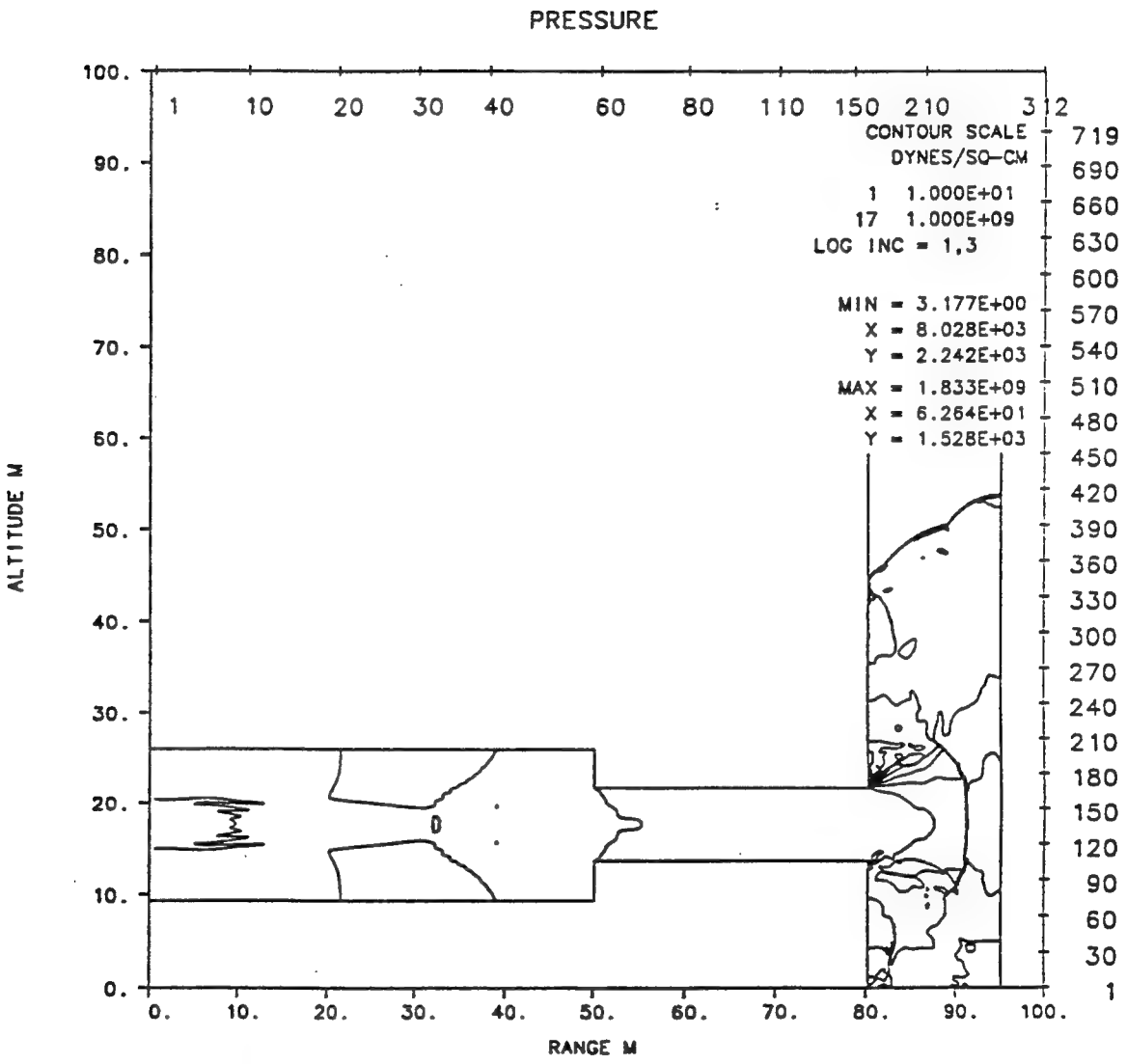

Figure 19. Pressure contour plot for two-dimensional Cartesian calculation at 25 ms.

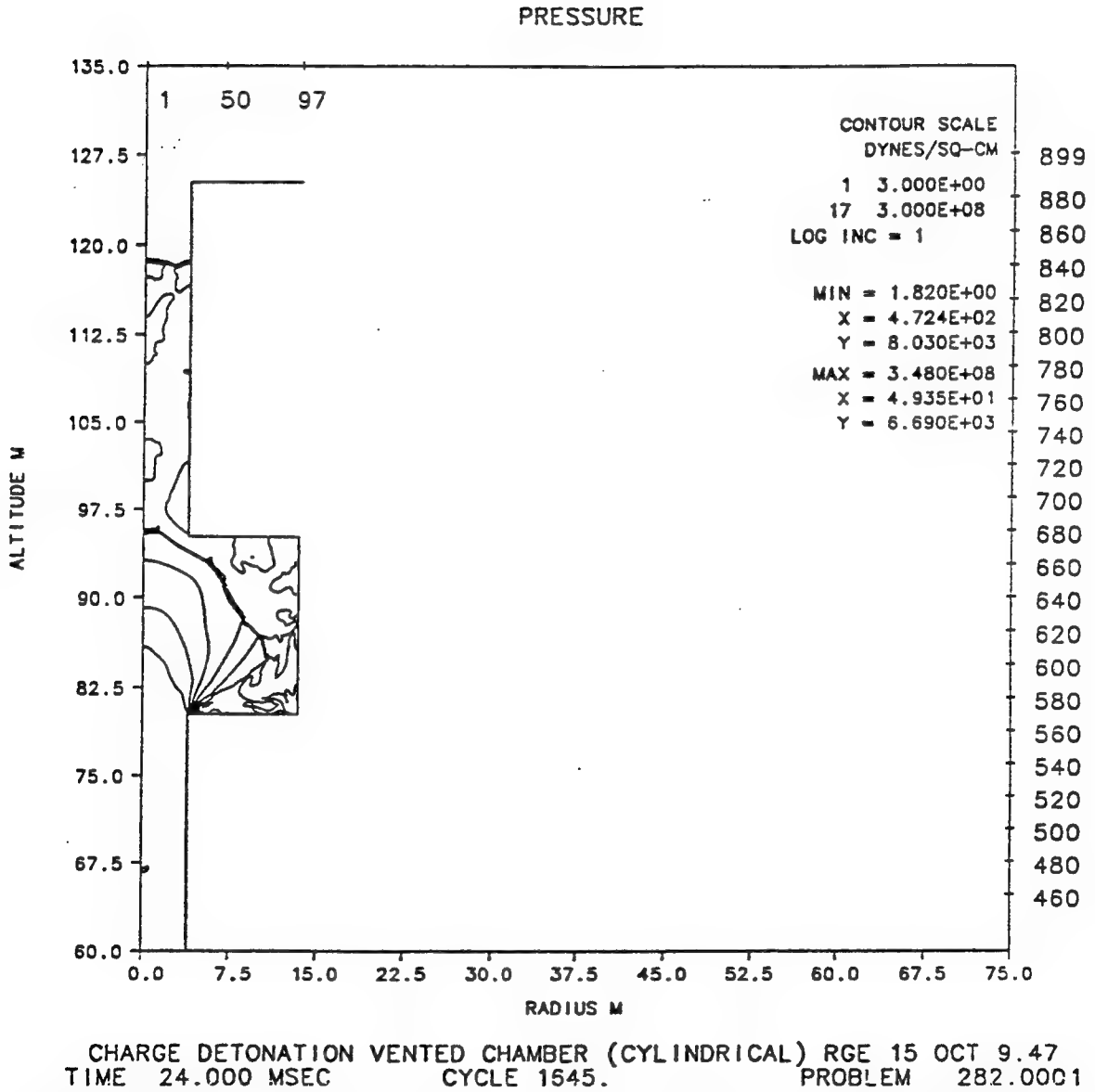

Figure 20. Pressure contour plot for two-dimensional cylindrical calculation at 24 ms.

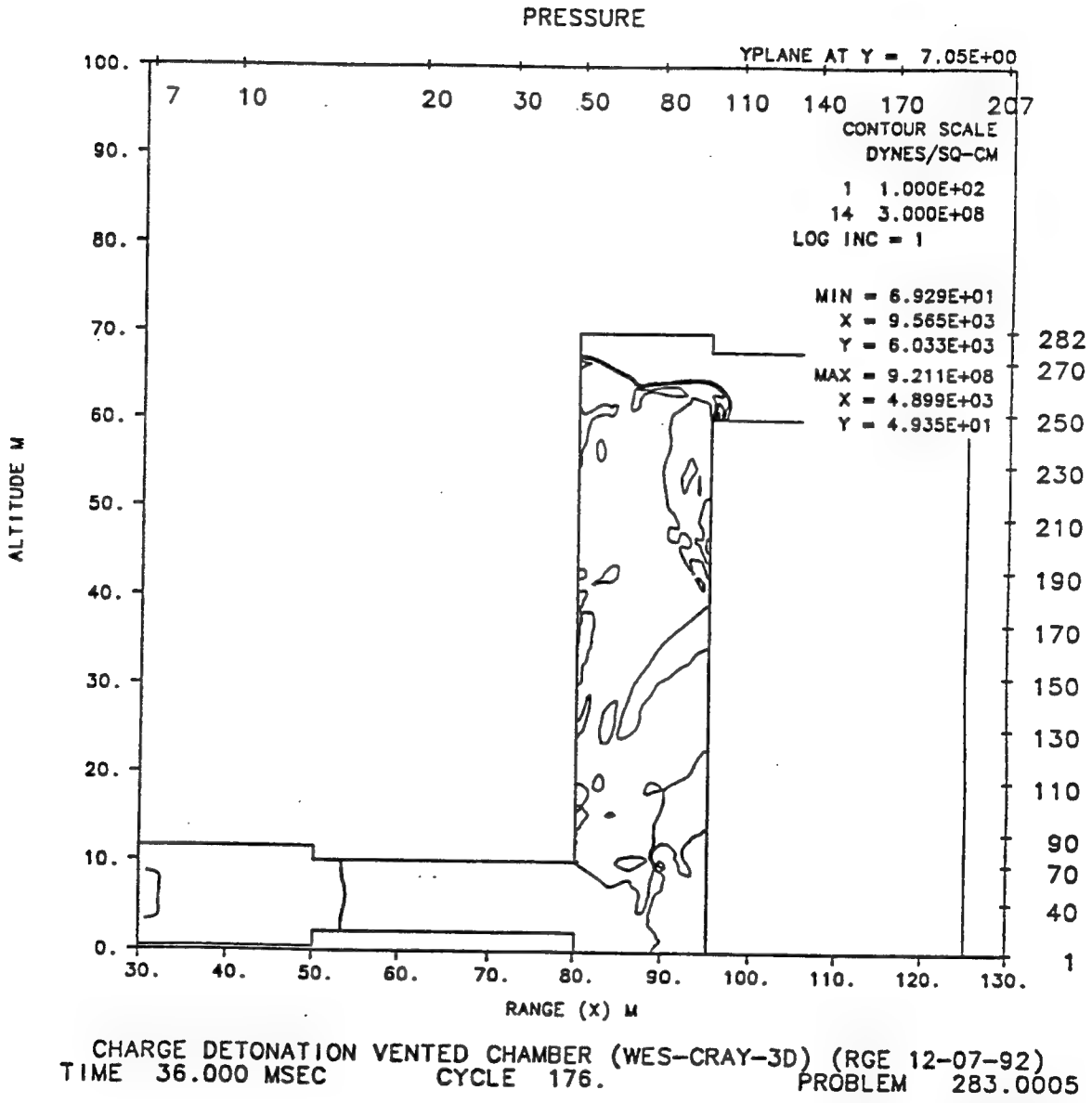

Figure 21. Pressure contour plot for three-dimensional Cartesian calculation at 36 ms.

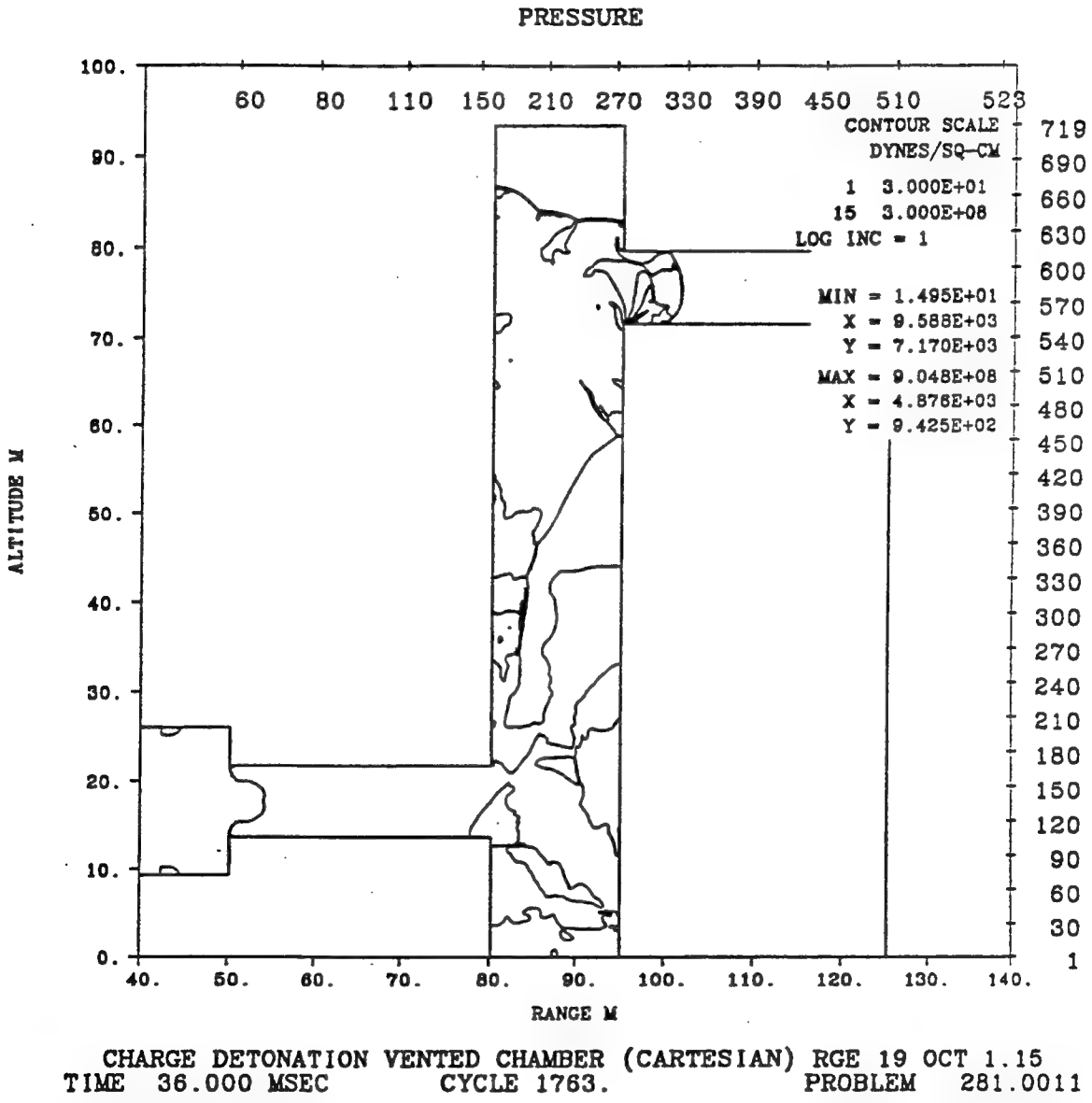

Figure 22. Pressure contour plot for two-dimensional Cartesian calculation at 36 ms.

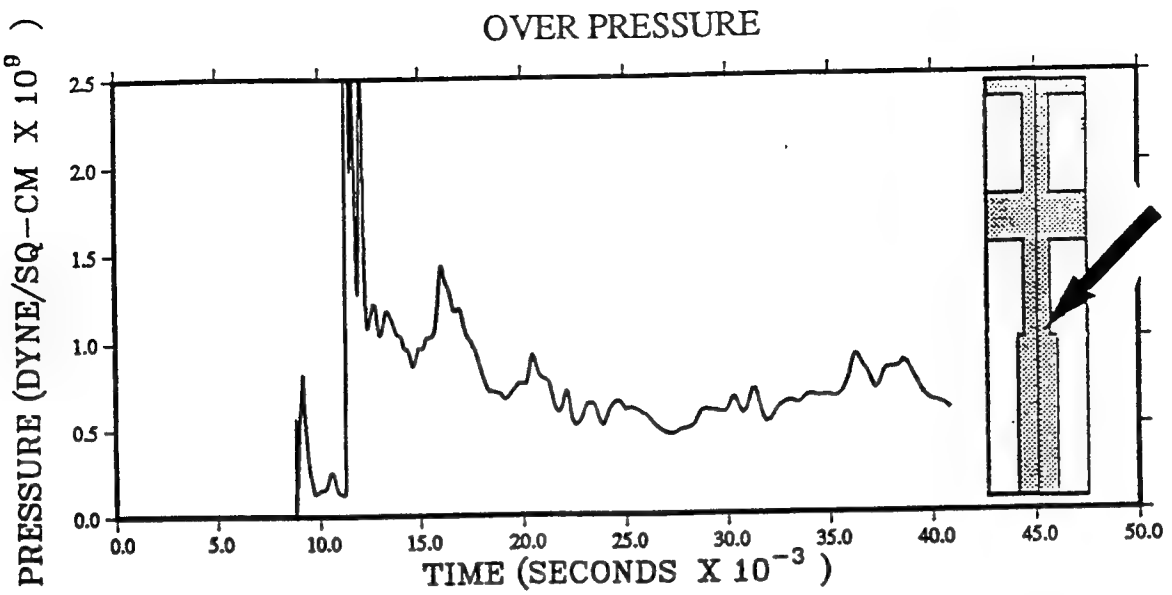

CHARGE DETONATION VENTED CHAMBER (CYLINDRICAL) RGE

282.0001.STA.9

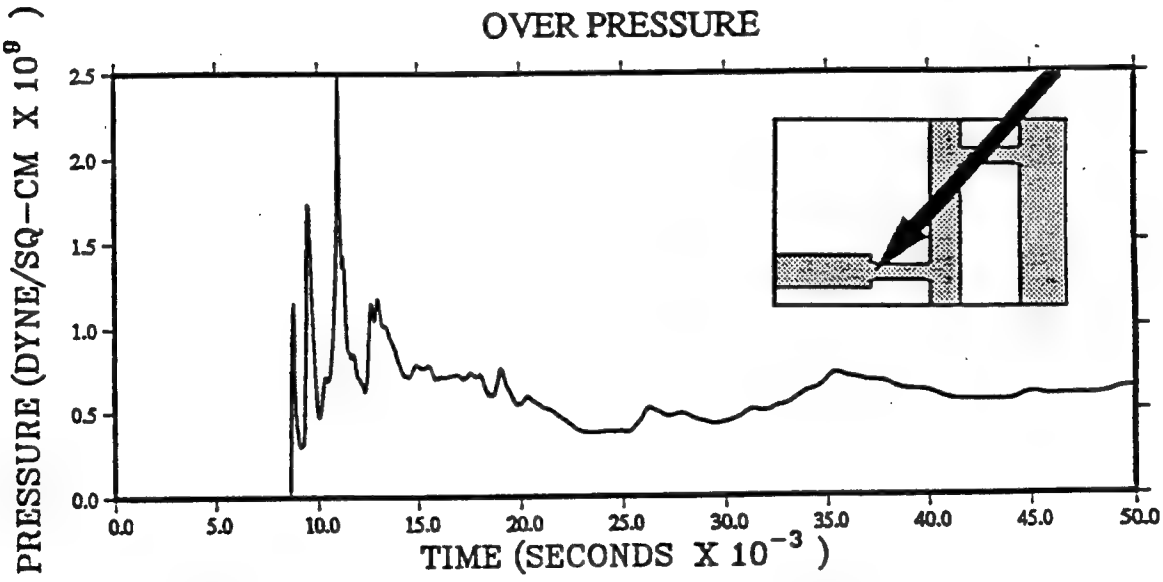

CHARGE DETONATION VENTED CHAMBER (CARTESIAN) RGE

281.0010.STA.9.CARTESIAN

Figure 23. Comparison of overpressure waveforms at entrance to input tube from two-dimensional (a) cylindrical and (b) Cartesian calculations.

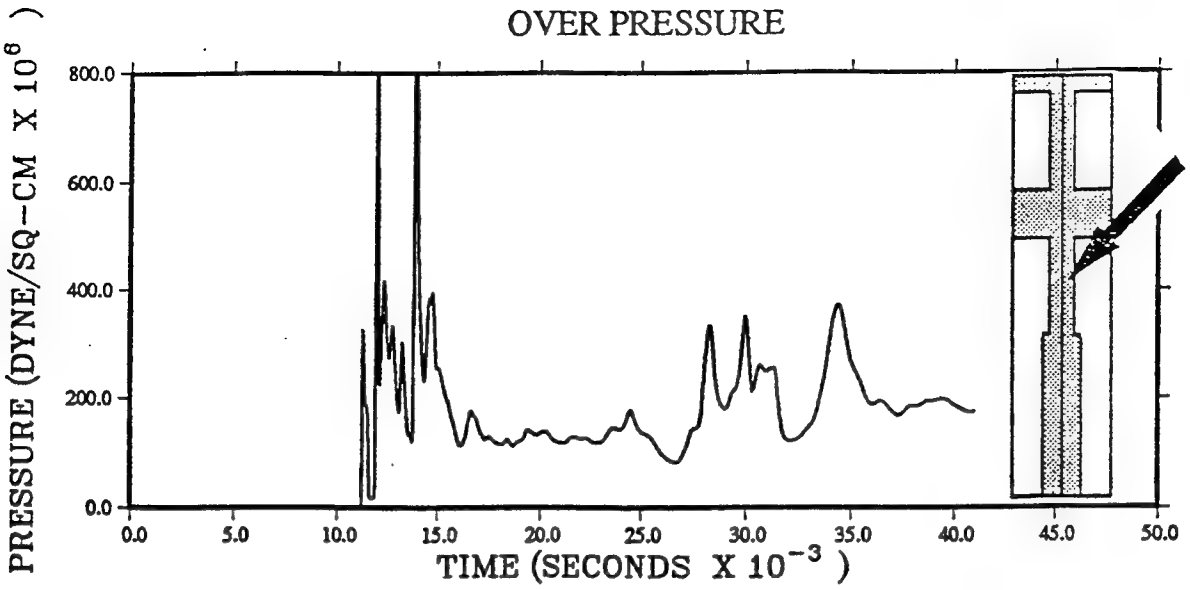

CHARGE DETONATION VENTED CHAMBER (CYLINDRICAL) RGE

282.0001.STA.21

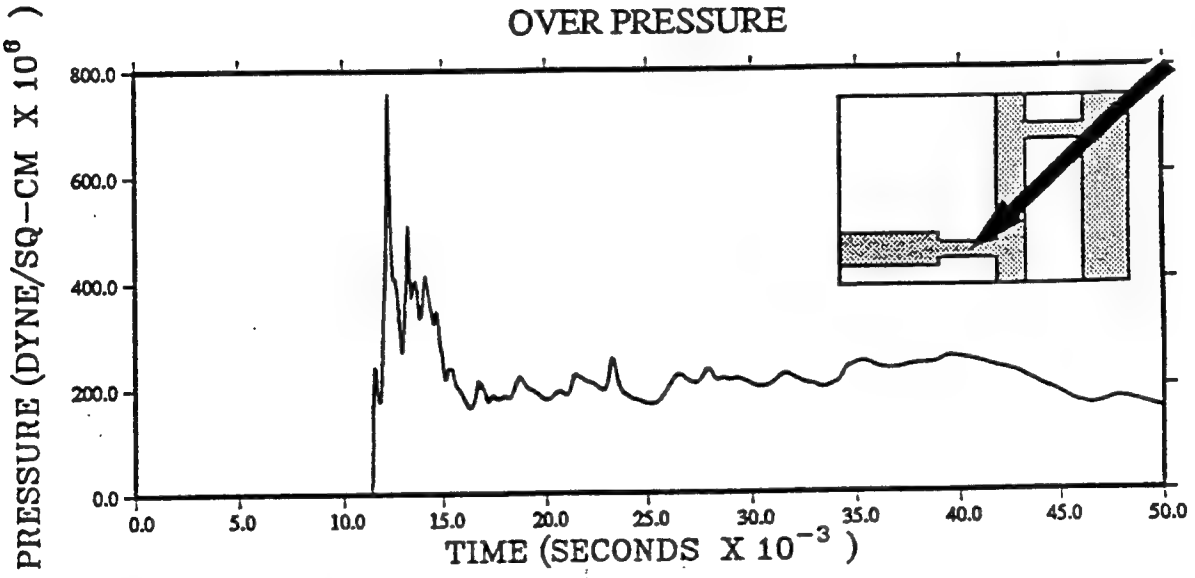

CHARGE DETONATION VENTED CHAMBER (CARTESIAN) RGE

281.0010.STA.10.CARTESIAN

Figure 24. Comparison of overpressure waveforms at center of input tube from two-dimensional (a) cylindrical and (b) Cartesian calculations.

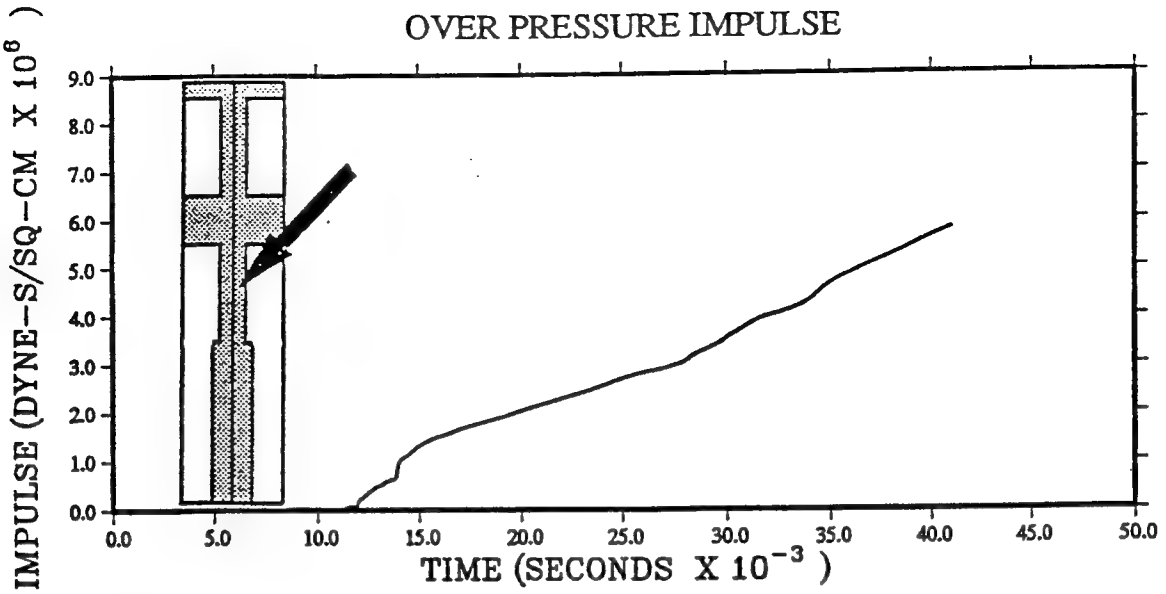

CHARGE DETONATION VENTED CHAMBER (CYLINDRICAL) RGE

282.0001.STA.21

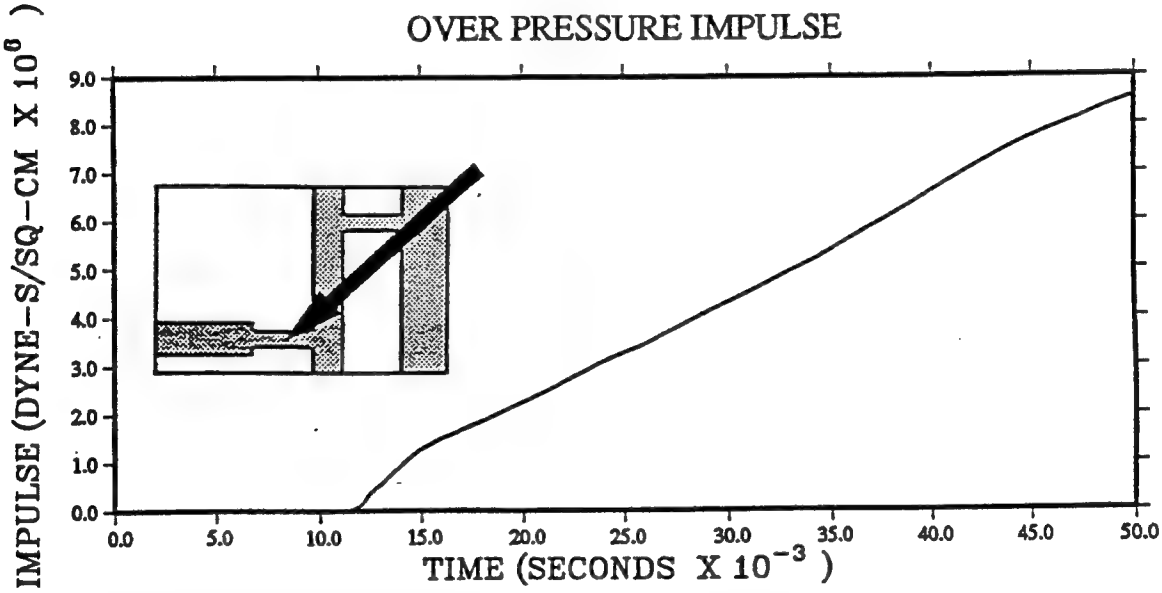

CHARGE DETONATION VENTED CHAMBER (CARTESIAN) RGE

281.0010.STA.10.CARTESIAN

Figure 25. Comparison of overpressure impulse records at center of input tube from two-dimensional (a) cylindrical and (b) Cartesian calculations.

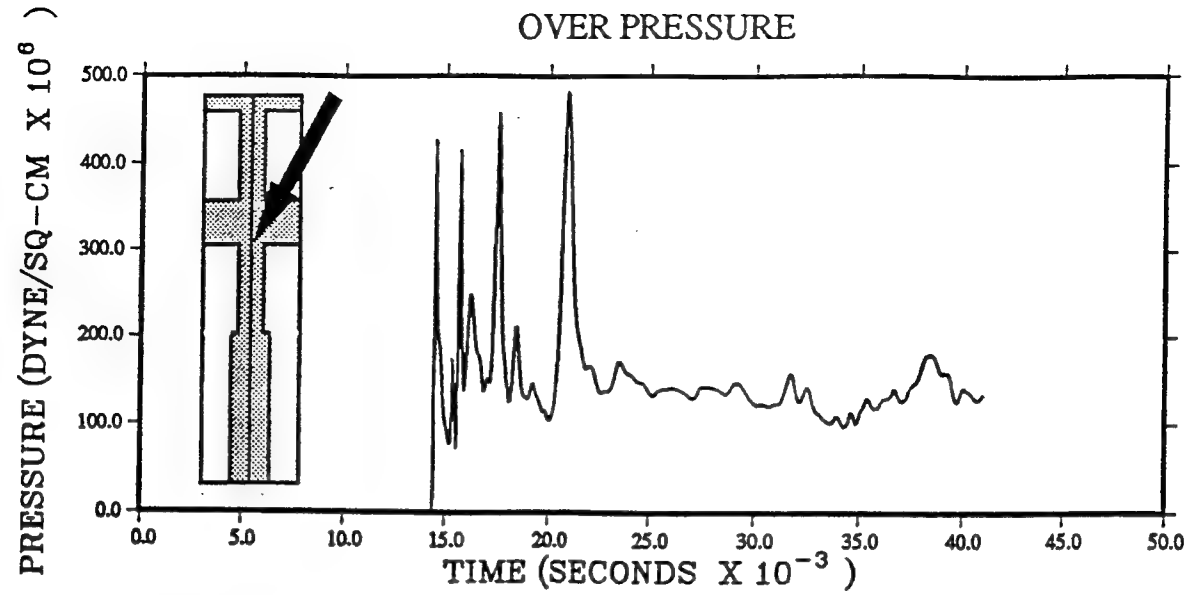

CHARGE DETONATION VENTED CHAMBER (CYLINDRICAL) RGE

282.0001.STA.25

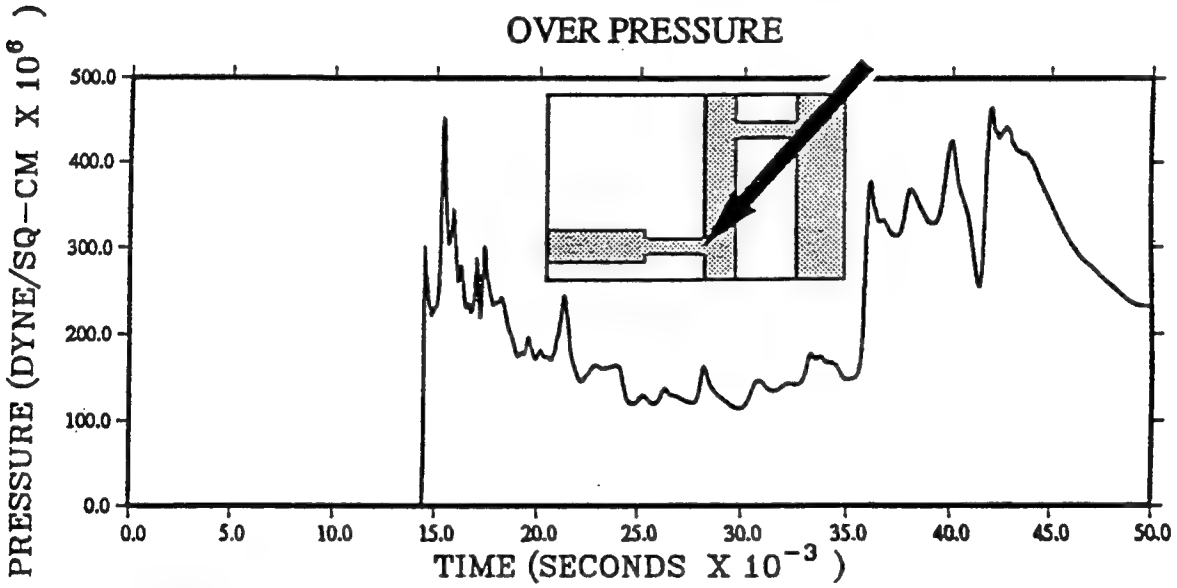

CHARGE DETONATION VENTED CHAMBER (CARTESIAN) RGE

281.0011.STA.11.CARTESIAN

Figure 26. Comparison of overpressure waveforms at entrance to expansion chamber from two-dimensional (a) cylindrical and (b) Cartesian calculations.

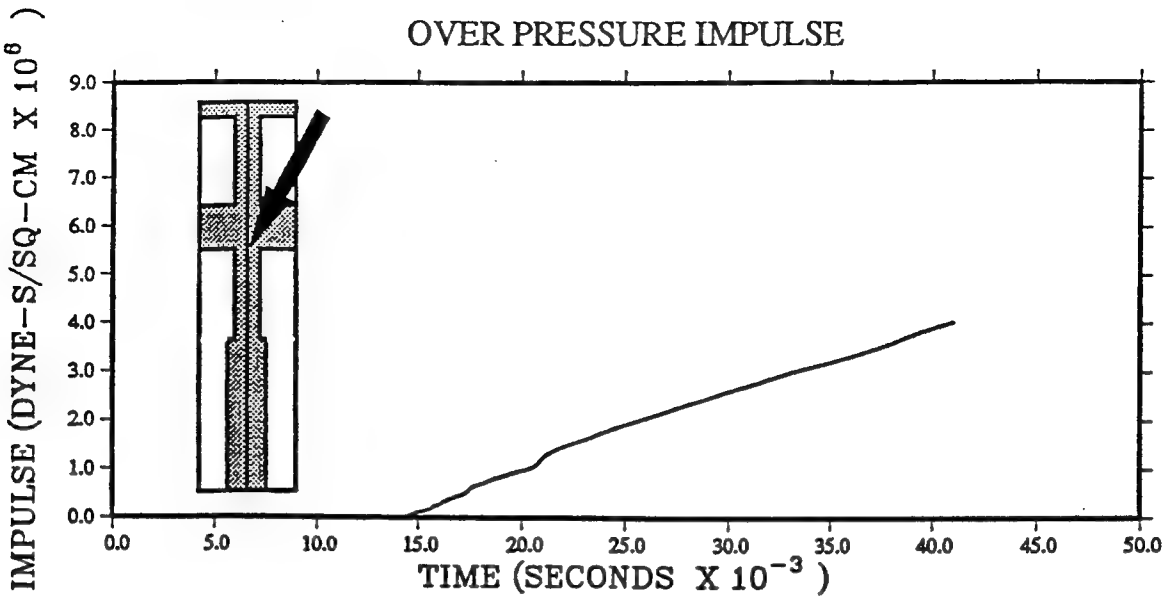

CHARGE DETONATION VENTED CHAMBER (CYLINDRICAL) RGE

282.0001.STA.25

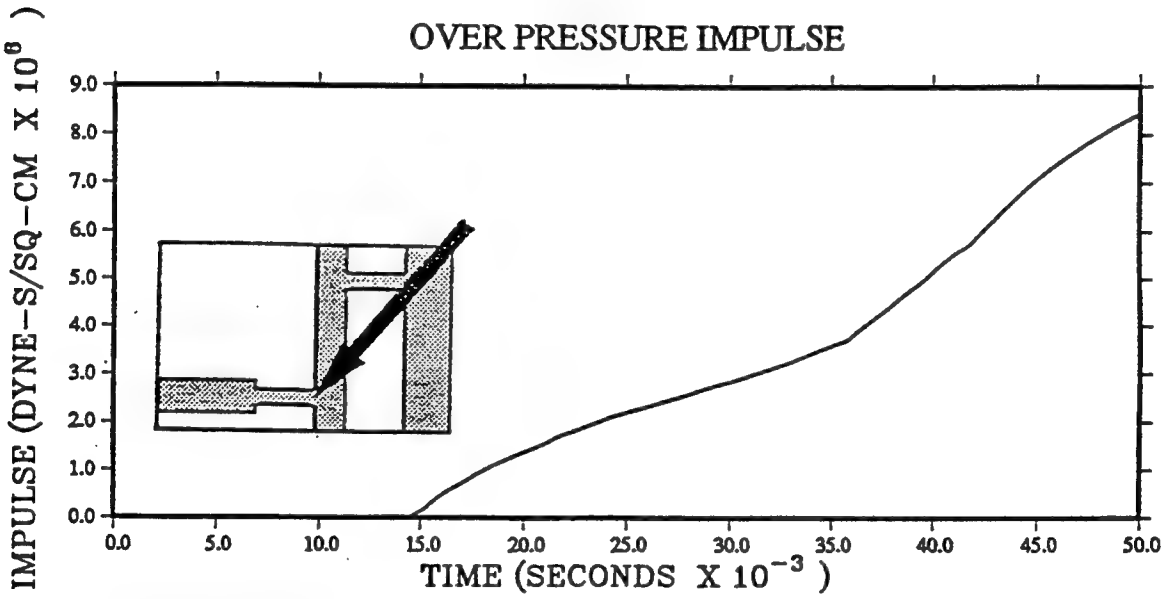

CHARGE DETONATION VENTED CHAMBER (CARTESIAN) RGE

281.0011.STA.11

igure 27. Comparison of overpressure impulse records at entrance to expansion chamber from two-dimensional (a) cylindrical and (b) Cartesian calculations.

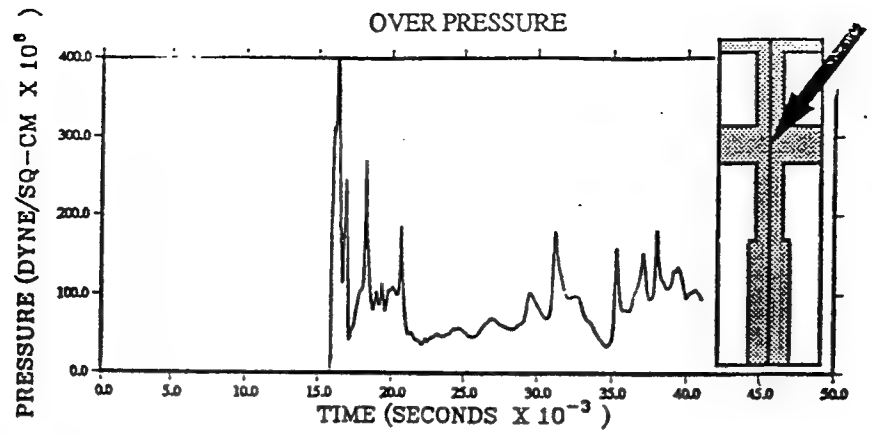

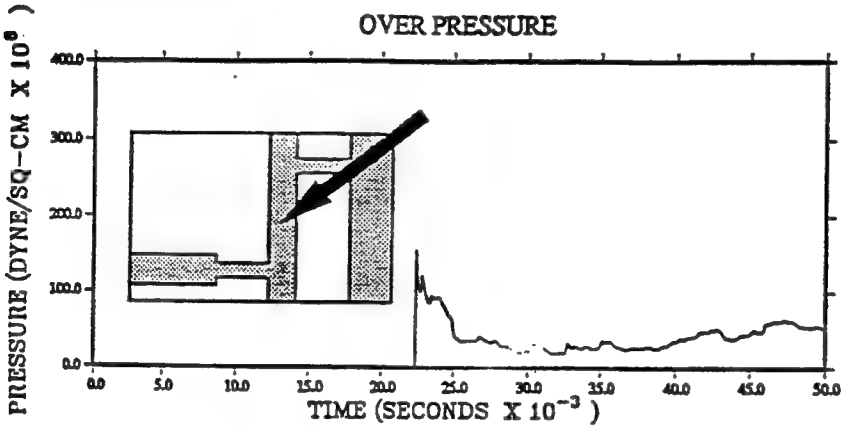

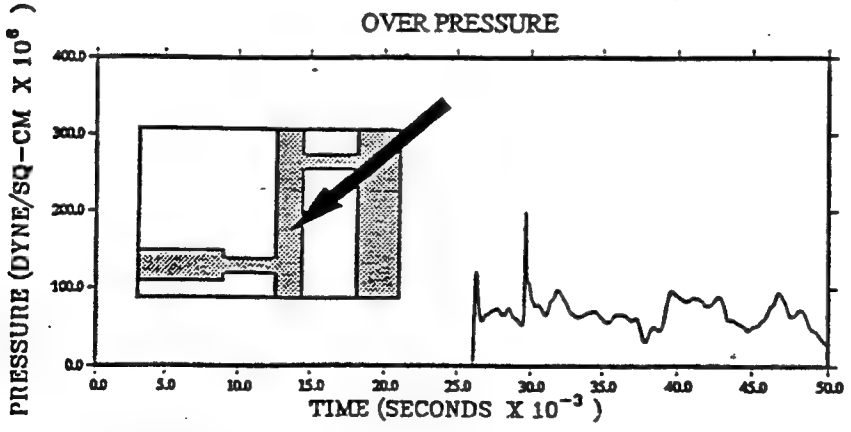

Figure 28. Comparison of overpressure waveforms at center of expansion chamber from two-dimensional (a) cylindrical and (b) Cartesian calculations, and from (c) three-dimensional Cartesian calculation.

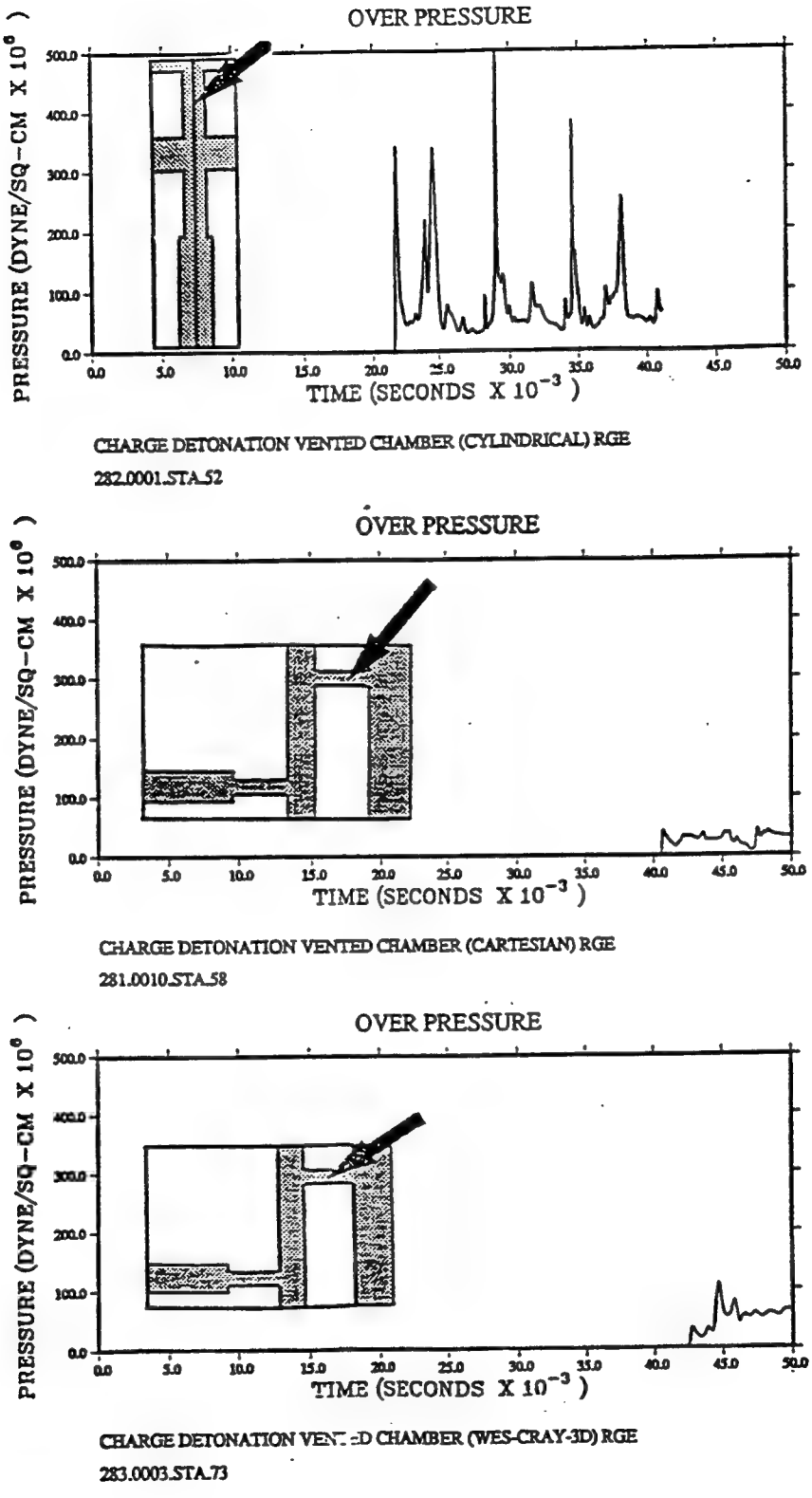

Figure 29. Comparison of overpressure waveforms at center of output tube from two dimensional (a) cylindrical and (b) Cartesian calculations, and from (c) three-dimensional Cartesian calculation.

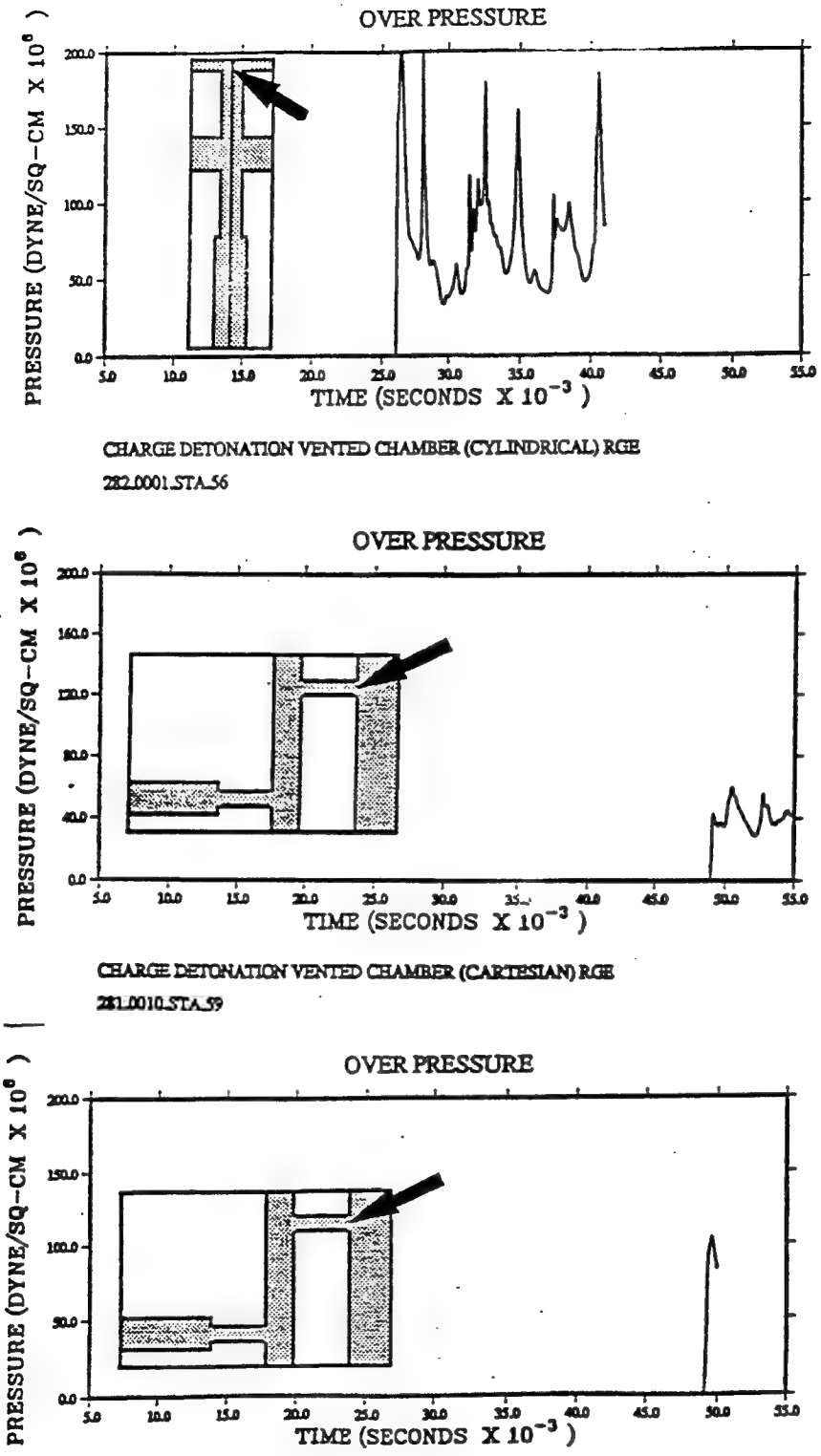

Figure 30. Comparison of overpressure waveforms at exterior end of output tube from two-dimensional (a) cylindrical and (b) Cartesian calculations, and from (c) three-dimensional Cartesian calculation.

SECTION 4

COMPARISON OF APPROACHES

4.1. Arrival Time, Peak Overpressure, and Peak Dynamic Pressure Comparisons

Figures 31, 32, and 33 are comparisons of arrival times, peak overpressures and peak dynamic pressures at selected points within the tunnel complex. For the independent variable, we use "cumulative distance," which is defined as the distance from the center back of the detonation chamber (the detonation point) along an orthogonal path to the point in question in the Cartesian cases. The path follows the centerline of the detonation chamber and input tube to the center of the expansion chamber at the input end. It then makes a right-angle turn and continues through the expansion chamber for the length of the input tube/output tube offset (58 m). A second right angle turn directs the path through the output tube to the portal. Key points on the cumulative distance path are given below:

Key Point on Cumulative Distance Path	Cumulative Distance to This Point
Detonation Chamber/Input Tube Interface	50.2 m
Input Tube/Expansion Chamber Interface	80.2 m
Center of Expansion Chamber at Input Tube End	87.7 m
Center of Expansion Chamber	116.7 m
Center of Expansion Chamber at Output Tube End	145.7
Expansion Chamber/Output Tube Interface	153.2 m
Portal	183.2 m

For the cylindrical results given in the plots, the independent variable has been adjusted so that key points in the cylindrical configuration are plotted at the corresponding points listed above. The cylindrical results are identical to those for the 3-D Cartesian results in the detonation chamber and input tube; thus only the 2-D and 3-D Cartesian results are plotted in this region.

The Cartesian arrival times, Figure 31, are in good agreement throughout the calculations. The 3-D shock is slightly later in the expansion chamber and beyond, probably because the higher overhead (8 m compared to the 6-m unit height in the 2-D case) allows more local expansion volume as the shock travels through the expansion chamber. The cylindrical case arrival time is much earlier, as expected, because of the shorter distance of travel to corresponding points in the complex.

The peak overpressure plot, Figures 32, shows similar values for the two Cartesian cases; however the 3-D values are slightly higher in all cases. This might be because the explosive detonation was better characterized by the axisymmetric representation. We expected the 2-D result to be almost the same as the 3-D during transition of the expansion chamber , but it never quite achieves the same amplitude. The cylindrical result is higher by nearly an order of magnitude because there are no right-angle turns to impede the flow.

This problem caused by unimpeded axial flow in the cylindrical case is particularly noticeable in Figure 33, in which peak dynamic pressures are plotted. For this plot, the dynamic pressure component shown for comparison was that in the primary direction of flow. For the cylindrical case, this was along the axial direction. For the Cartesian configurations, we used the horizontal (in the previously described calculational representation) component within the detonation chamber and input and output tubes, the vertical component in the expansion chamber. Because there is crossflow in all the chambers, this may not have been the best choice, and may be responsible for the erratic behavior of the curves.

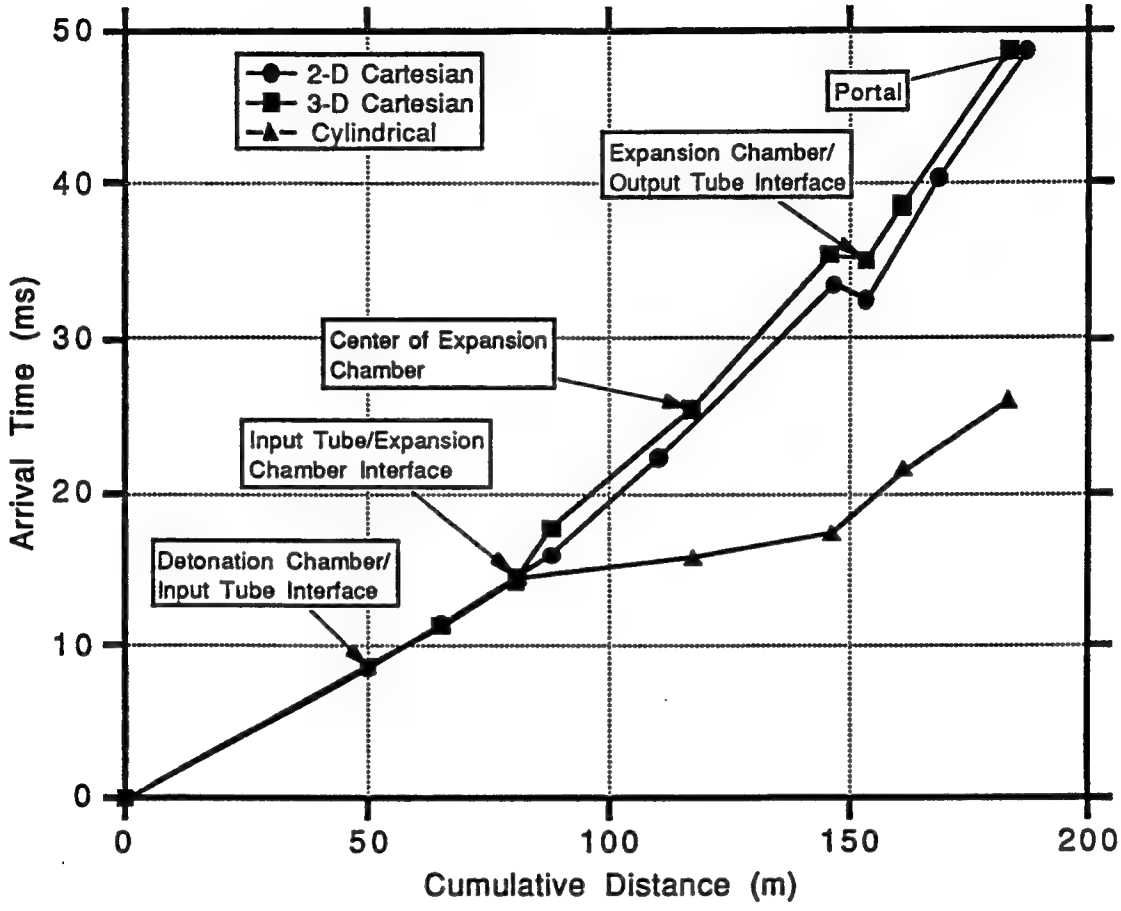

Figure 31. Arrival time comparison for the three configurations along an orthogonal central path from detonation point to portal.

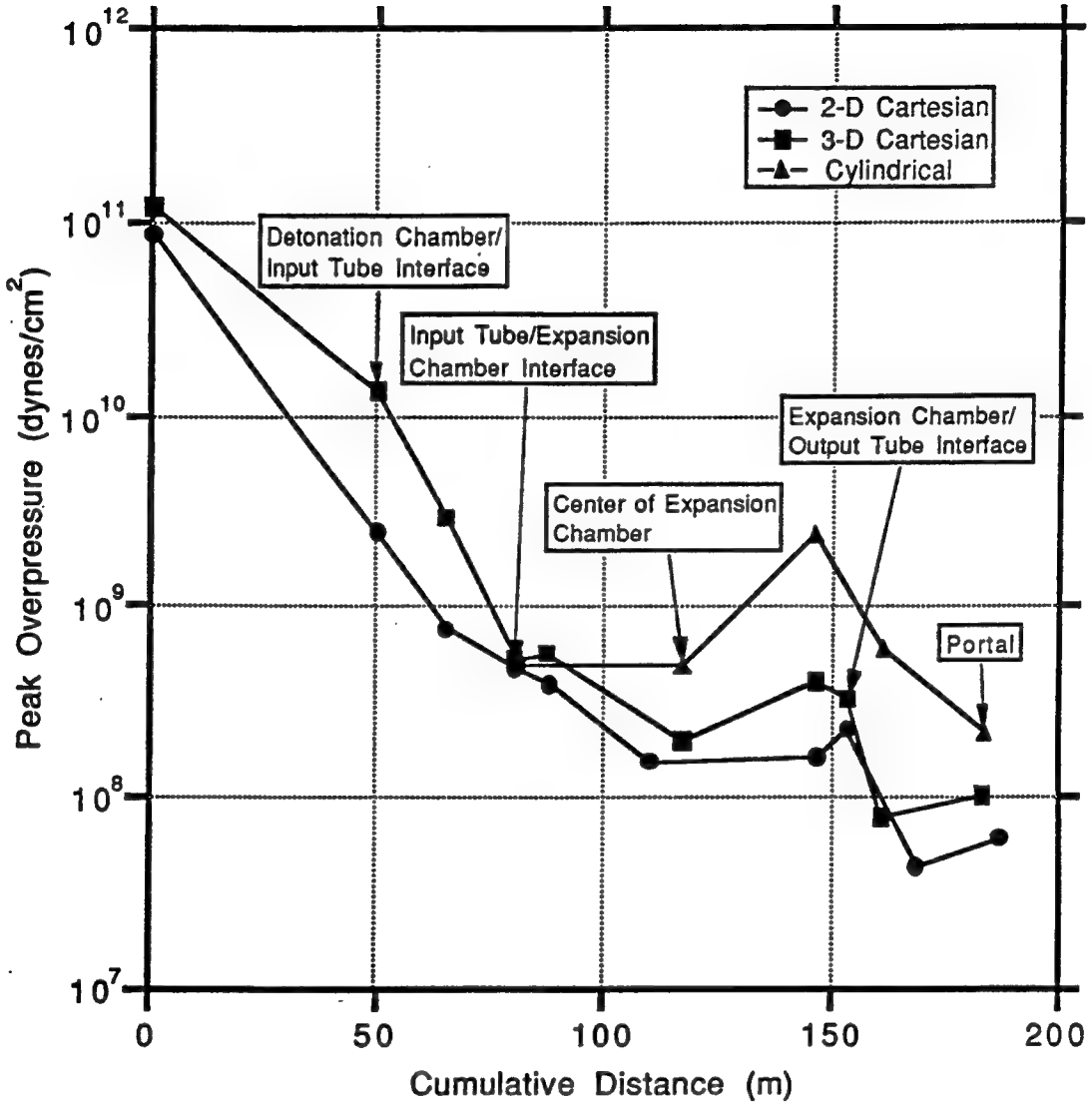

Figure 32. Peak overpressure comparison for the three configurations along an orthogonal central path from detonation point to portal.

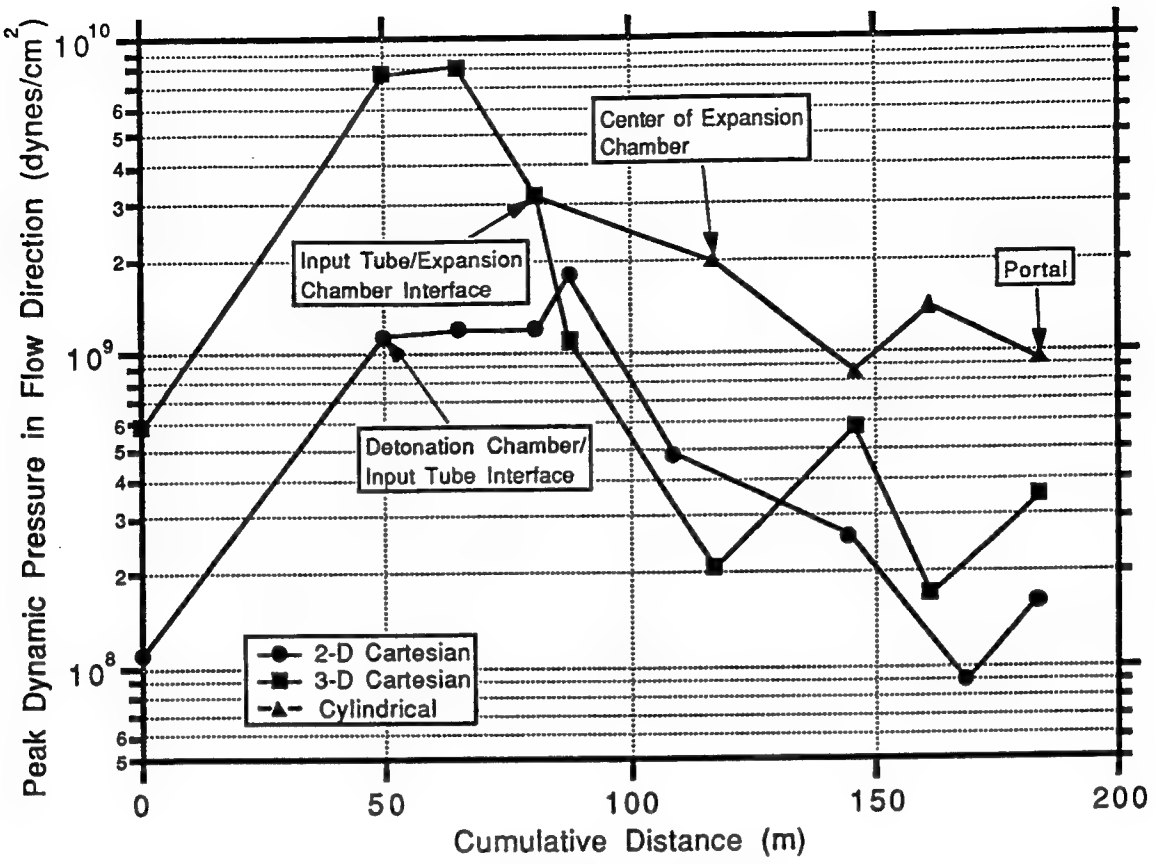

Figure 33. Peak dynamic pressure (in primary flow direction) for the three configurations along an orthogonal central path from detonation point to portal.

4.2. Discussion

The three geometric representations were shown approximately in Figure 1, and in more detail in the subsequent figures. The three-dimensional case has a cross-section reduction between the detonation chamber and connecting tunnel (or input tube), a significant expansion in cross section and a right-angle turn upon transition to the expansion chamber, a travel distance of 58 m before another right-angle turn and a cross-section reduction to the output tube. The two-dimensional cylindrical approximation includes the appropriate cross-sectional area changes but has no changes of direction. The total length of the expansion chamber, as traversed by the shock wave, is considerably shorter in the cylindrical than in the other cases. Therefore we expected, and observed, reduced arrival times in the cylindrical case. Because there were no changes in direction, the dynamic pressures were significantly higher than in either of the Cartesian cases.

This lack of direction changes was also a factor contributing to the reduced arrival times.

In the 2-D Cartesian case, the right-angle turns and the distance between turns was accurately represented. The detonation chamber, originally cylindrical, was modified to equalize its volume. Also, the expansion chamber shape was modified. The cross-sectional area of the expansion chamber, for a plane normal to the major flow direction, was somewhat less than in the true, 3-D geometry. The resulting difference in volume was accounted for by extending the expansion chamber equally on each side beyond the input and output tube connections. These changes account for the differences noted in these regions. Because the volumes, distances and angles in the 2-D and 3-D Cartesian cases are nearly equal, the results from the two calculations at the portal are reasonably close.

SECTION 5
CONCLUSIONS AND RECOMMENDATIONS

In this study, we set up the same basic situation in three different calculational configurations, performed the calculations, and then compared results to determine whether a two-dimensional approximation is valid to represent a three-dimensional problem, and if so, whether a cylindrical or Cartesian representation most nearly reproduces the true three-dimensional result. The answer is, and this might have been expected, that any time a change is made to the configuration, this change will be reflected to some degree in the emerging waveform. Ideal surfaces reflect shocks, and if these surfaces are at different distances from the source, or are oriented differently, then the reflected waves, as they contribute to the form of an out-flowing wave, will arrive at different times and have different characteristics. This cannot be avoided.

In many cases, however, the exact waveform to be observed at some point within or just outside of a tunnel complex is not as important as the peak overpressure, peak dynamic pressure, or their respective impulse values. In these cases, two-dimensional representations, if they are carefully done, can provide adequate predictions of test cases or adequate simulations for detonation scenarios of interest.

A three-dimensional simulation gives, of course, the closest correspondence to the desired situation. This must be balanced by the fact that the third dimension may require one to two orders of magnitude more computing time, because the computer is doing the equivalent of a number of two-dimensional calculations equal to the number of cells in the third direction. A large, fast, mainframe computer is usually required to complete a three-dimensional calculation, and these are not always readily available. A compromise is often reached by using a coarser mesh size, which may or may not be appropriate, depending on requirements of the calculational results.

Based on the results of this study, it appears that a two-dimensional Cartesian representation is a reasonable choice for most tunnel configurations which include corners around which the shock wave must flow. Such a configuration provides a reasonably accurate simulation of the actual interior, although problems may arise, for example, if the explosive charge is fairly small so that stretching it over the whole unit height makes it ridiculously narrow. It has been our experience that a charge which is less than about five computational cells wide will not burn properly, because of the pressure release at the edges.

The cylindrical configuration is not really appropriate for configurations with corners like the one of interest here. The path that the shock wave follows in the cylindrical case is a straight shot along the centerline; it is not degraded by bouncing off of walls as it goes around corners. The path lengths are not correct, so the times-of-arrival are not correct. This configuration should provide a "worst-case" answer, but it may be too conservative in many instances.

While analyzing the results of the cylindrical calculation, we thought of a modification that might be incorporated into the configuration to provide a better simulation. This consists of placing a "blocker" in the expansion chamber on the centerline to break up the flow, as shown in Figure 34. The outer diameter of the expansion chamber would have to be modified slightly to maintain the appropriate expansion chamber volume, and the size of the blocker could be modified to control total path length, and hence arrival time of the shock at the exit tunnel. Care would need to be taken not to choke the flow by making the entrance and exit to the expansion chamber smaller in the cross section than the entrance and exit tubes themselves.

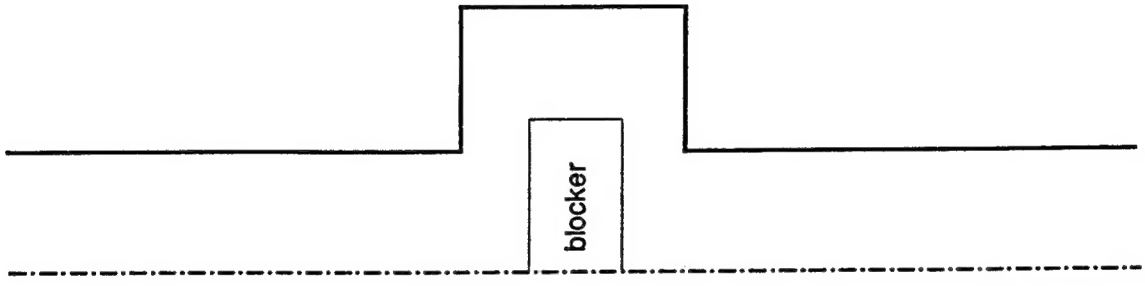

Figure 34. Cylindrical expansion chamber configuration with "blocker".

The Cartesian two-dimensional calculation could also have been set up in a slightly different manner which, in retrospect, might have been more realistic. Referring to Figure 3, recall that the "length" of the expansion chamber, shown as the horizontal dimension in the figure, was actually the shortest dimension of the chamber. This was held constant, while the "width" (shown vertically) was adjusted to maintain the appropriate volume. This approach required the addition of alcoves at the sides of the expansion chamber whose ends were farther from the entrance and exit tunnels than those in the three-dimensional configuration, and hence modified the timing of waves reflected from the side walls. Another approach would have been to maintain the width constant, and to make an adjustment in the length of the expansion chamber. This modification is illustrated in Figure 35, which shows the changes to the expansion chamber shape in

heavy dashed lines. The "width" (vertical) of the expansion chamber is maintained at 70 m, while the "length" (horizontal) is increased to 20 m to accommodate the 6-m unit height. The volume is the same in both cases.

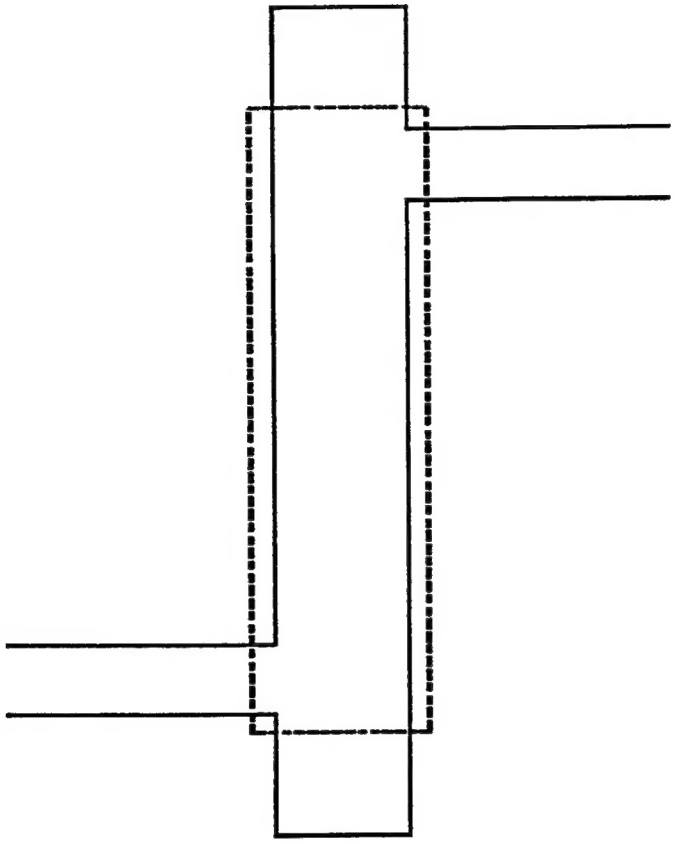

Figure 35. Expansion chamber in two-dimensional Cartesian system illustrating a possible modification to the chamber shape.

REPORT DOCUMENTATION PAGE

Form Approved
OMB No. 0704-0188

1.AGENCY USE ONLY *(Leave blank)*	2.REPORT DATE	3.REPORT TYPE AND DATES COVERED
	September 1995	Final report

4.TITLE AND SUBTITLE
Influence of Geometric Approximations on Computational Results in Complex Tunnel Configurations

5.FUNDING NUMBERS
DACA39-92-R-0063

6.AUTHOR(S)
Robert G. Ekler, Lynn W. Kennedy, Charles E. Needham

7.PERFORMING ORGANIZATION NAME(S) AND ADDRESS(ES)
S-Cubed, A Division of Maxwell Laboratories
2501 Yale Boulevard, SE, Suite 300
Albuquerque, NM 87106

8.PERFORMING ORGANIZATION REPORT NUMBER
SSS-DFR-93-13838
UAST-CR-93-002

9.SPONSORING/MONITORING AGENCY NAME(S) AND ADDRESS(ES)
U.S. Army Engineer Waterways Experiment Station
3909 Halls Ferry Road
Vicksburg, MS 39180-6199

10.SPONSORING/MONITORING AGENCY REPORT NUMBER
Contract Report SL-95-7

11.SUPPLEMENTARY NOTES
Available from National Technical Information Service, 5285 Port Royal Road, Springfield, VA 22161.

12a.DISTRIBUTION/AVAILABILITY STATEMENT
Approved for public release; distribution is unlimited.

12b.DISTRIBUTION CODE

13.ABSTRACT ***(Maximum 200 words)***

Three calculational representations of a tunnel/expansion chamber complex were set up and calculations were run using the hydrocode SHARC. The three representations included a two-dimensional azisymmetric (cylindrically symmetric) configuration, a two-dimensional Cartesian configuration, and a three-dimensional Cartesian. Each representation includes an explosive in a detonation chamber, an input tunnel, an expansion chamber, and an output tunnel connecting to the exterior. Approximations necessary to describe the tunnel complex in these representations are discussed.

Results from the three calculations are compared under the assumption that the three-dimensional configuration most closely approximates a real-life test situation. The accompanying discussion provides and compares alternatives for representing a tunnel in various coordinate systems for calculational simulation.

14.SUBJECT TERMS

Airblast calculations	Hydrocodes	Two-dimensional
Calculational approximations	SHARC	
High-explosive simulations	Three-dimensional	

15.NUMBER OF PAGES
58

16.PRICE CODE

17.SECURITY CLASSIFICATION OF REPORT	18.SECURITY CLASSIFICATION OF THIS PAGE	19.SECURITY CLASSIFICATION OF ABSTRACT	20.LIMITATION OF ABSTRACT
UNCLASSIFIED	UNCLASSIFIED		